TASC
THE ANALYTIC SCIENCES CORPORATION

MAGSAT INVESTIGATION OF CRUSTAL MAGNETIC ANOMALIES IN THE EASTERN INDIAN OCEAN

Richard V. Sailor
Andrew R. Lazarewicz
The Analytic Sciences Corporation
One Jacob Way
Reading, Massachusetts 01867

February 22, 1983
Final Report for Period December 1980 — February 1983

Prepared For:

NATIONAL AERONAUTICS AND SPACE ADMINISTRATION
Goddard Space Flight Center
Greenbelt, Maryland

Technical Report Documentation Page

1. Report No.	2. Government Accession No.	3. Recipient's Catalog No.

4. Title and Subtitle
Magsat Investigation of Crustal Magnetic Anomalies in the Eastern Indian Ocean

5. Report Date
22 February 1983

6. Performing Organization Code

7. Author(s)
R.V. Sailor, A.R. Lazarewicz

8. Performing Organization Report No.
TASC-TR-1325-1

9. Performing Organization Name and Address
The Analytic Sciences Corporation
One Jacob Way
Reading, Massachusetts 01867

10. Work Unit No. (TRAIS)

11. Contract or Grant No.
NAS5-26424

12. Sponsoring Agency Name and Address
Dr. Robert A. Langel, Code 922
NASA Goddard Space Flight Center
Greenbelt, Maryland 20771

13. Type of Report and Period Covered
Final Report
Dec. 1980 - Feb. 1983

14. Sponsoring Agency Code

15. Supplementary Notes

16. Abstract

Crustal magnetic anomalies in a region of the eastern Indian Ocean have been studied using data from NASA's Magsat mission. The investigation region (0 deg to 50 deg South, 75 to 125 deg East) contains several important tectonic features, including the Broken Ridge, Java Trench, Ninetyeast Ridge, and Southeast Indian Ridge. A large positive magnetic anomaly is associated with the Broken Ridge and smaller positive anomalies correlate with the Ninetyeast Ridge and western Australia.

The investigation first considered individual profiles of scalar data (computed from vector components) to determine the overall data quality and resolution capability. Spectrum analysis indicates that anomaly features with wavelengths shorter than 250 km are not resolved. Spectral coherence analysis of closely-spaced tracks shows that magnetic anomaly features with wavelengths longer than 700 km are repeatable from track to track.

After these assessments of data resolution capability, a set of Magsat "Quiet-Time" data was used to compute an equivalent source crustal magnetic anomaly map of the study region. Maps of crustal magnetization and magnetic susceptibility were computed from the equivalent source dipoles. Gravity data were used to help interpretation, and a map of the ratio of magnetization to density contrasts was computed using Poisson's relation. The results are consistent with the hypothesis of induced magnetization of a crustal layer having varying thickness and composition.

17. Key Words	18. Distribution Statement
Magsat Crustal Magnetic Anomalies Indian Ocean Broken Ridge Ninetyeast Ridge	PRECEDING PAGE BLANK NOT FILMED

19. Security Classif. (of this report)	20. Security Classif. (of this page)	21. No. of Pages	22. Price
UNCLASSIFIED		88	

PREFACE

Satellite observations of the earth's magnetic field have resulted in improved models for the earth's main field, better observations of time-varying and external field effects, and mapping (on a consistent global basis) of the long-wavelength component of crustal magnetic anomalies. The Magsat mission, which spanned a period of seven months from November 1979 to June 1980, was the first to carry both vector and scalar magnetometers. It successfully completed all of its major objectives, and provided data from altitudes as low as 250 km. One of the major contributions of Magsat to global geophysics is the extensive data set that has permitted the mapping of crustal magnetic anomalies. These large-scale magnetic anomalies are still not fully understood, but further progress will be made as analysis progresses on the data from Magsat and subsequent missions.

The present investigation has been concerned with crustal magnetic anomalies in a marine area. The main objectives were to evaluate the quality of Magsat data and to produce and interpret crustal magnetic anomaly maps of the eastern Indian Ocean. That region was selected because of the presence of significant tectonic features and a significant positive magnetic anomaly that was recognized over Broken Ridge by earlier investigators using POGO satellite data.

Proper interpretation of satellite magnetic observations begins with understanding the data collection and reduction process, and especially by determining how the resolution of the observations is limited by noise and other factors. Because of the attenuation of the magnetic field with increasing altitude, the presence of external and time-varying field components, and the effects of instrument noise and spacecraft motion, crustal anomaly features with wavelengths shorter than some cutoff value will not be observable. Determination of this resolution limit for Magsat data for the eastern Indian Ocean was made by spectrum analysis of individual data profiles. The main conclusions from the analysis of individual tracks of Magsat data crossing the eastern Indian Ocean are:

- Major magnetic anomaly features are correlated with tectonic features
- Magnetic anomaly spatial wavelengths shorter than 250 km are not observable in Magsat data because of noise
- For pairs of closely-spaced tracks of Magsat data, features with wavelengths longer than 700 km are repeatable from track to track.

These results, concerning data quality, data preprocessing, and analysis of individual anomaly profiles are discussed in Chapters 2 and 3.

The information on data quality and resolution capability helped direct the two-dimensional map analysis that followed. A map of crustal magnetic anomalies for the eastern Indian Ocean was made from the data designated by NASA as "quiet-time" (generally free of external field disturbances). This map was constructed using the Equivalent Source modeling software provided by NASA. In this procedure, a grid composed of dipoles aligned parallel to the earth's main magnetic field is used to represent the magnetized crustal layer. The dipole moment for each of the equivalent sources is computed by a least-squares fit to the observations. This correctly accounts for variations of satellite altitude. Since this technique does suffer from edge effects at the boundaries of the dipole grid, a set of sixteen equivalent source solutions for different overlapping sub-regions of the study area were computed. These were combined to form a final set of solution dipoles covering the central 40 deg × 40 deg portion of the study area. The solution dipoles were used to produce a magnetic anomaly map (reduced-to-the-pole) for an altitude of 350 km. This altitude is approximately the average altitude of the Magsat mission and has been used by other investigators for crustal anomaly maps. In addition to producing a map of magnetic anomaly, the solution dipoles were also used to produce maps of crustal magnetization and susceptibility. These maps are described in Chapter 4.

The final stage of this investigation was geophysical interpretation of the map products that

were developed from Magsat data. Maps of bathymetry and gravity anomaly were used to show the correlation between magnetic and tectonic features. A quantitative merging of the magnetic and gravity data was done using Poisson's relation. This relation, based on the assumptions of uniform density and magnetization, allows computation of the ratio between the magnetization and density contrasts. This was done by dividing the reduced-to-the-pole magnetic field map by a map of the vertical gradient of gravity at an altitude of 350 km. The resulting map for the eastern Indian Ocean has nearly constant values over most of the region, suggesting that Poisson's relation is applicable over most of the area. However, an exception to this rule is a long linear trend that parallels to the south of the Diamantina Fracture Zone and cuts across the boundary between the Broken Ridge and Ninetyeast Ridge.

The main conclusions from the map analysis and geophysical interpretation are:

- Significant positive crustal magnetic anomalies are associated with Broken Ridge, Ninetyeast Ridge, and western Australia
- The western and eastern parts of Broken Ridge have different characteristics for both gravity and magnetic anomalies
- Positive crustal magnetic anomalies may be associated with thicker crust
- Results are consistent with a hypothesis of induced magnetization of a crust of varying thickness and composition.

The consistency with the hypothesis of induced magnetization is based on the fact that reduction-to-the-pole gives reasonable results. The competing hypothesis of remanent magnetization has not yet been ruled out. These results are discussed in Chapter 5 while Chapter 6 is a summary of the report.

Recommendations for further work include additional analysis of correlations between the magnetic and gravity fields to determine the depth of

sources for both types of anomaly. This should be done in both the spatial and frequency domains.

ACKNOWLEDGMENTS

Drs. Robert F. Brammer, Stephen L. Baumgartner, and James V. White provided guidance and assistance throughout this investigation. Dr. Robert A. Langel of NASA Goddard Space Flight Center provided much technical information and data. The Magsat data of Dr. Langel were provided by the National Space Science Data Center. Dr. Richard H. Rapp of The Ohio State University provided gravity data.

TABLE OF CONTENTS

LIST OF FIGURES

LIST OF FIGURES (Continued)

LIST OF FIGURES (Continued)

LIST OF TABLES

1. INTRODUCTION

1.1 BACKGROUND AND OBJECTIVES

The TASC Magsat Investigation covers an area in the eastern Indian Ocean that contains several major bathymetric and tectonic features (Figs. 1-1 and 1-2). The overall objectives of this investigation are:

- Determination of the resolution of Magsat data and the optimum grid spacing for magnetic anomaly maps of the study region
- Production of magnetic anomaly maps from Magsat data covering the study region (0-50 deg S, 75-125 deg E)
- Comparison of Magsat and gravity field data in the area, and quantification of their relationships
- Interpretation of the Magsat data using satellite altimeter and other geophysical data in order to determine the origin of the observed magnetic anomalies.

The investigation area contains a variety of tectonic and physiographic features as shown in Fig. 1-1. The most prominent features include the Southeast Indian Ridge, the Ninetyeast Ridge, Broken Ridge, Wharton Basin, Java Trench, and Diamantina Fracture Zone. Since the tectonic histories of the Ninetyeast Ridge and Broken Ridge are still controversial, any new information that can be gained from satellite magnetic observations will be valuable. For example, a global magnetic anomaly map prepared from POGO data (Ref. 1) showed a significant magnetic high over the Broken Ridge. This anomaly feature

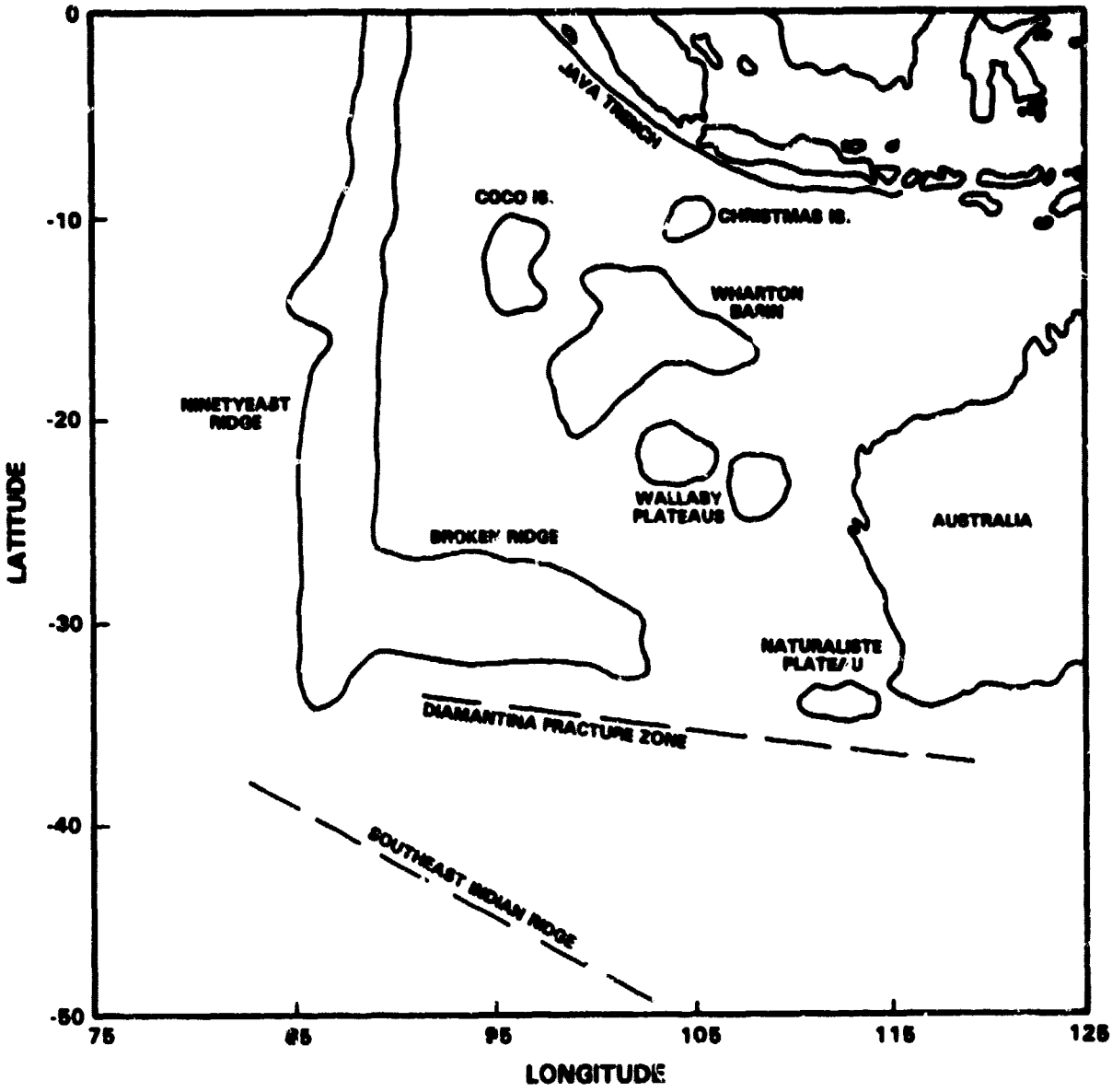

Figure 1-1 Tectonic features of investigation region

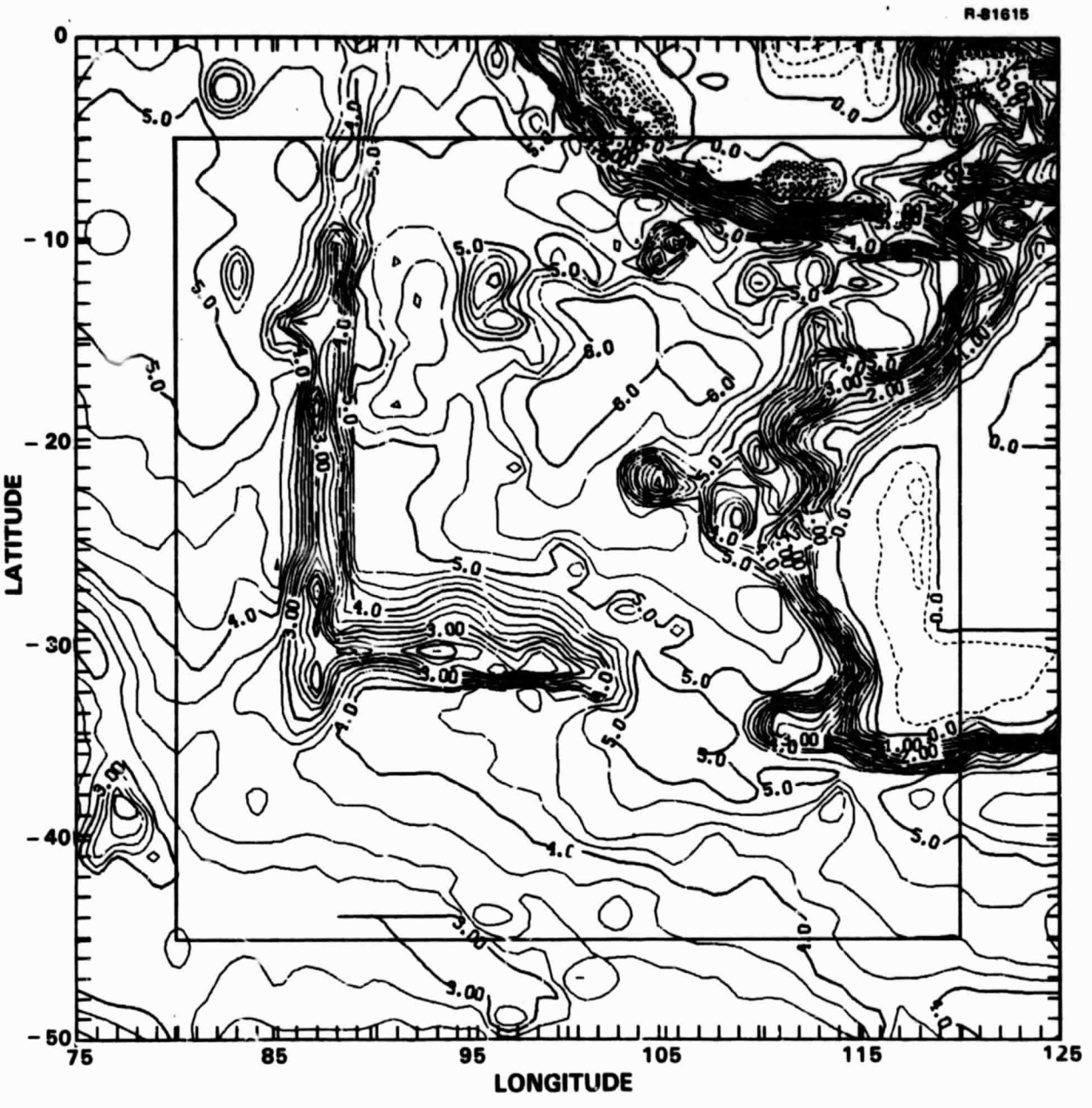

Figure 1-2 Bathymetry (in km) of investigation region. Inset box is area covered by final magnetic anomaly map.

might be cited as evidence indicating the presence of continental crust at Broken Ridge. (See Chapter 5 for more discussion of Broken Ridge.) By using gravity data to supplement the Magsat magnetic anomaly observations, the present study

has achieved better interpretations than would be possible using only one of these data types.

1.2 OVERVIEW OF THIS REPORT

This report summarizes the TASC Magsat investigation of crustal magnetic anomalies in the eastern Indian Ocean. Chapter 2 begins with a brief description of the Magsat data that was provided by NASA GSFC. This chapter also describes the initial assessments of data quality and the steps of data preprocessing that were performed in order to analyze the crustal magnetic anomalies.

In Chapter 3, the analysis of crustal magnetic anomalies begins with examples of the anomaly features that are observed along individual Magsat passes. These one-dimensional studies enabled the resolution capability of the fundamental data products to be determined, that is, how well can the Magsat Investigator-B data resolve crustal magnetic anomaly features. The data profiles do reveal significant anomaly features associated with Broken Ridge, Java Trench, and the Southeast Indian Ridge. These features are consistent from track-to-track, although they are distorted by the long-wavelength effects of the external field, and by short wavelength noise. Thus, an important question concerns the separation of the crustal anomaly field from the external field and from other noise sources. The approach of this chapter is to consider this question in the frequency domain, that is, to determine the frequency bands over which noise dominates and over which the crustal anomaly signal is dominant. The approach is to compute power spectral density (PSD) estimates from the Magsat data and to compare these with the spectra that are expected to result from crustal magnetic anomalies. The noise contribution to the data PSD

was identified by analysis of nearly repeating passes of Magsat data. This was done in the frequency domain by computing the spectral coherence between pairs of Magsat tracks which have nearly the same geographic location. The results of these computations indicate that for wavelengths less than about 700 km, the Magsat data is not repeatable from track-to-track. This chapter concludes with a review of the characteristics of Magsat data in several different frequency bands.

Chapter 4 describes the two-dimensional (map) analysis of crustal magnetic anomalies. The chapter begins with a discussion of the data resolution and the effect that this has upon the accuracy of two dimensional maps. The Magsat tracks covering the study area are used in an equivalent source inversion to produce a map of crustal magnetic anomalies. The results of this are also shown for a separate portion of the study area surrounding Broken Ridge. The equivalent source technique also was used to construct maps of relative magnetization and relative magnetic susceptibility of the crust.

Chapter 5 is devoted to geophysical interpretation of the Magsat results. Additional data sources, including gravity anomaly and bathymetry have been compiled for the study area. Poisson's relation, an analytic relationship between the potentials of the gravity and magnetic anomaly fields, is used to relate the gravity and the Magsat observations.

Chapter 6 discusses the final results and presents the summary, conclusions, and recommendations for further research.

2. DATA PREPROCESSING AND QUALITY ASSESSMENT

2.1 MAGSAT DATA SOURCES

NASA GSFC has released two main types of data products for the Magsat mission: 1) CHRONICLE data includes all magnetometer measurements (at a data rate of 16 samples/sec for vector measurements) plus ephemeris information. 2) INVESTIGATOR-B data has been reduced in sampling rate to one sample every five seconds (by averaging over 80 observations), contains values predicted by a core field model, values of magnetic activity indices, and is available for specified geographical regions. These data types are described further in a NASA Technical Memorandum (Ref. 2).

The results shown in this report are based mainly on the Investigator-B data, limited to the eastern Indian Ocean (Investigation region defined by Fig. 1-1). For the production of the magnetic anomaly maps, TASC used only those orbits designated as "Quiet-Time" by NASA -- 631 passes crossing the investigation region between November 2, 1979 and May 17, 1980.

2.2 DATA QUALITY AND PREPROCESSING

Before large scale processing of Magsat data can be accomplished, it is necessary to evaluate the data quality and determine what preprocessing, if any, is required. Optimum computational methods and parameters (e.g., the minimum spacing for equivalent source dipoles) can then be determined. This

section will discuss the effects of data preprocessing on spectrum results. The two main areas of data preprocessing are: 1) correction of spikes and data gaps, and 2) subtraction of linear trends to reduce external field noise.

For the analysis of along-track data, 24 revs crossing the region without major data gaps were selected from the Investigator-B tapes. The data quantities used were the scalar magnitude computed from vector components using the 80-point average. Figure 2-1 shows the locations of some of these tracks. All revs had 180 points or fewer, and none had fewer than five missing points (flagged with 99999.0). In order to maintain a uniformly spaced data series, the actual value of the missing points must be estimated and inserted into the time series. For this analysis, linear interpolation was used to estimate the missing data values. After subtracting field values predicted by a 13th order field model, MGST(4/81-2), spikes of up to 15 nT were found to contaminate the residual time series (Fig. 2-2). It is likely that these smaller spikes are noise, as their spatial wavelengths are shorter than the resolution limit for the data (Section 3.4).

These small spikes and areas of increased high frequency noise are an important aspect of data quality. For the purpose of identifying noisy portions of data, it seemed appropriate to first look at the standard deviation of the 80-point running average, which is provided on the Investigator-B tapes. However, as Fig. 2-3 shows, this quantity mainly reflects the field gradient since the field changes significantly in the ~36 km interval over which the 80 observations are averaged. Thus, this quantity would not be useful, except for identifying only the largest spikes. Discussions with Dr. Langel led to the suggestion by TASC that this standard deviation quantity be replaced on future Investigator tapes, as it is not

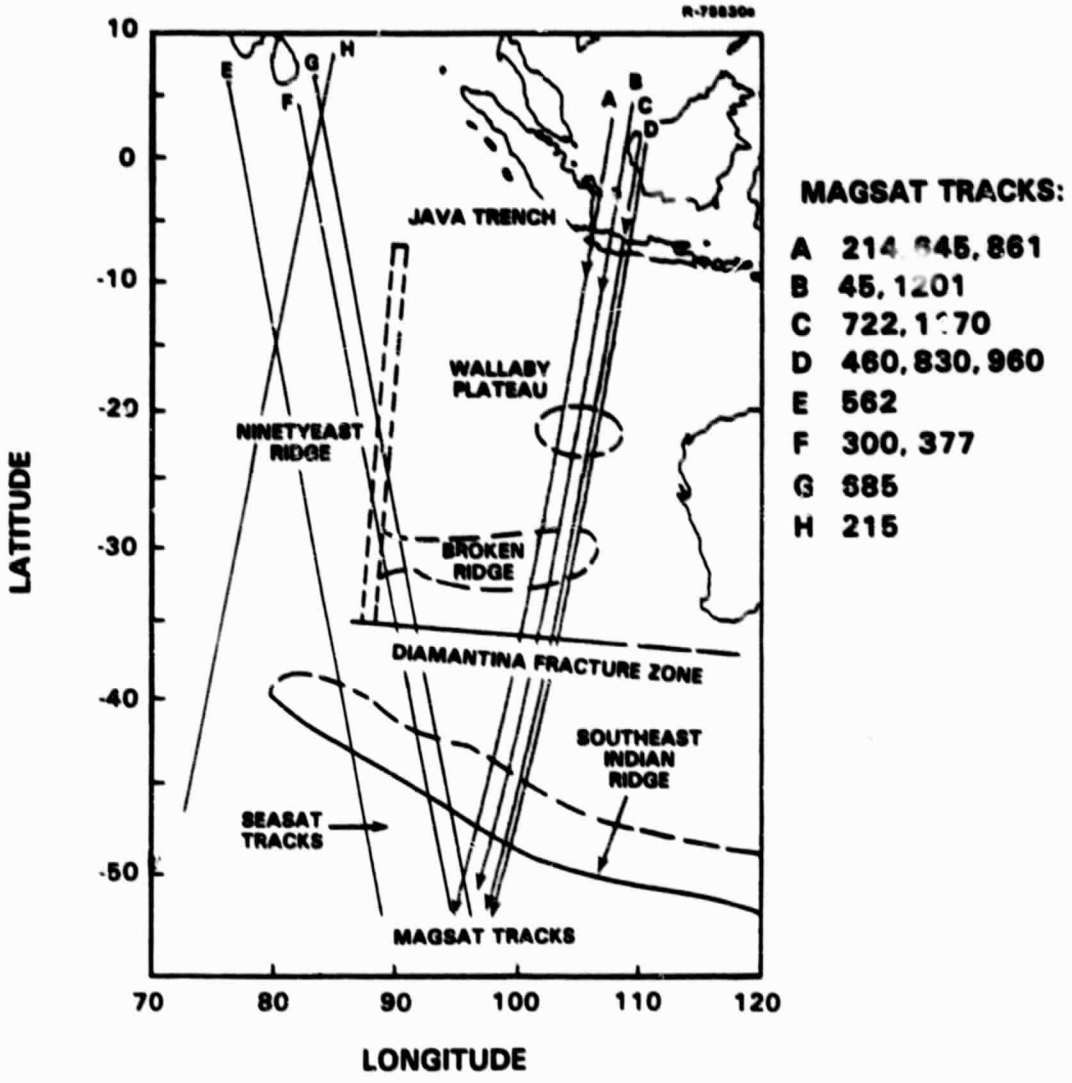

Figure 2-1 Investigation region with selected Magsat tracks

useful for showing short-wavelength noise. For example, for Rev 45, the field gradient in the Z component is large, and the standard deviation of the averages has the form of a ramp, with the standard deviation ranging from about 120 to 5 nT.

A more useful quantity for study of the quality of the Magsat data is formed by subtracting the 80-point running average from the observed values. This is plotted in

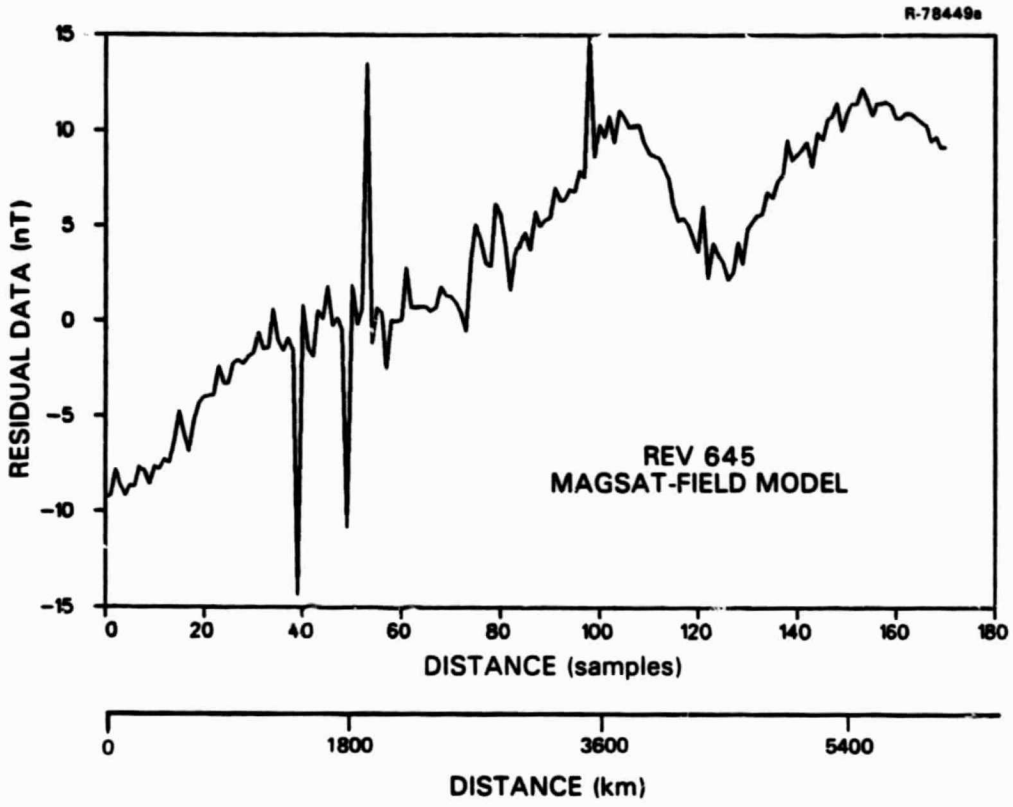

Figure 2-2 Rev 645 scalar magnitude data minus MGST(4/81-2) field model. The 8 to 15 nT data spikes are noise in the Magsat data

Figs. 2-4 and 2-5, which show this quantity to be much less sensitive to the field gradient and shows more clearly the data spikes and the areas which are more noisy. Analysis of this quantity (e.g., computing running averages over several points) could be used to identify and correct spikes. Further development of such a procedure is recommended for future studies. For the remainder of the present investigation, spikes were identified and removed using a five-point running average on the anomaly profiles: a data point with value more than three standard deviations away from the running mean was replaced by the value of that mean. The averaging interval was automatically changed if several spikes or data gaps were within the interval.

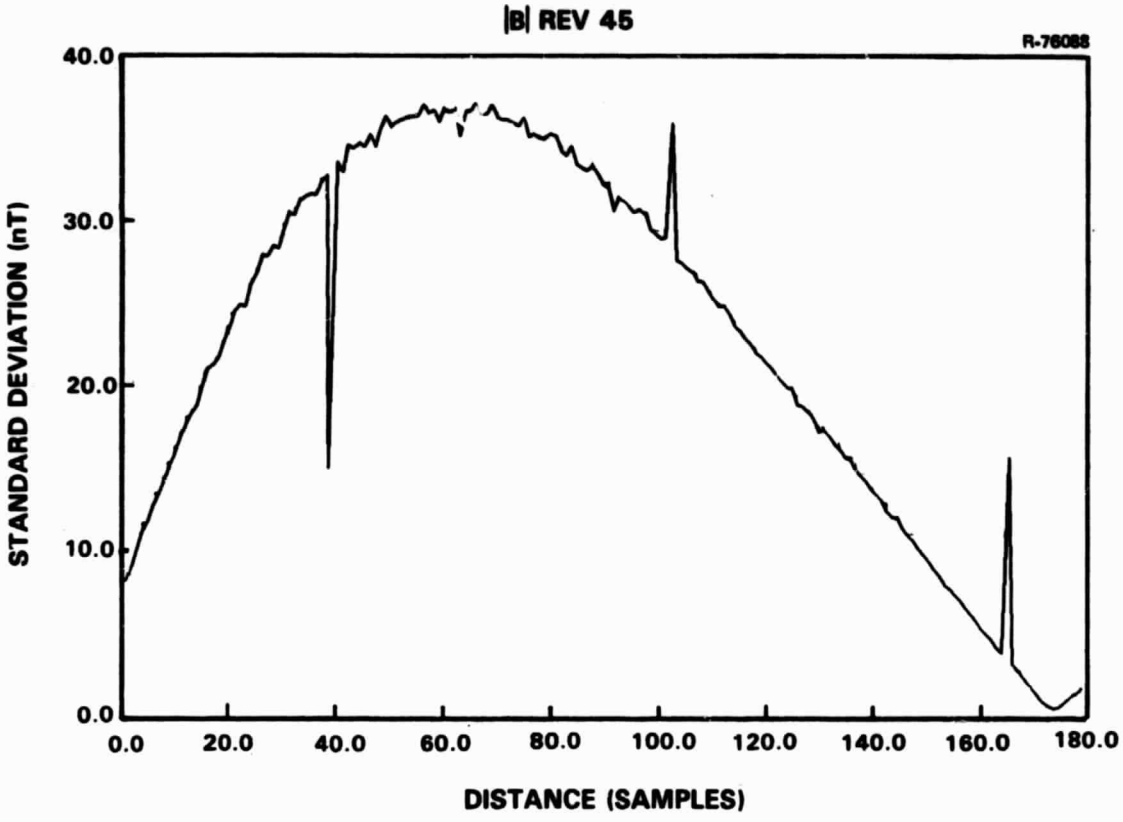

Figure 2-3 Standard deviation of the running average over 80 observations

Effective analysis of crustal anomaly fields requires a knowledge of both the wavelength passband which contains the desired geophysical information and the effective passband where sufficient information exists in the data. Knowledge of these passbands will permit determination of the optimum spacing for the grid of equivalent dipole sources. As a first step in defining these passbands, the effects of ramp removal on spectral estimates will be shown.

The first stage of data reduction for the study of crustal magnetic anomalies is the subtraction of the effects of the core field. Subtracting a field model of degree and order 13 removes wavelengths longer than about 3000 kilometers.

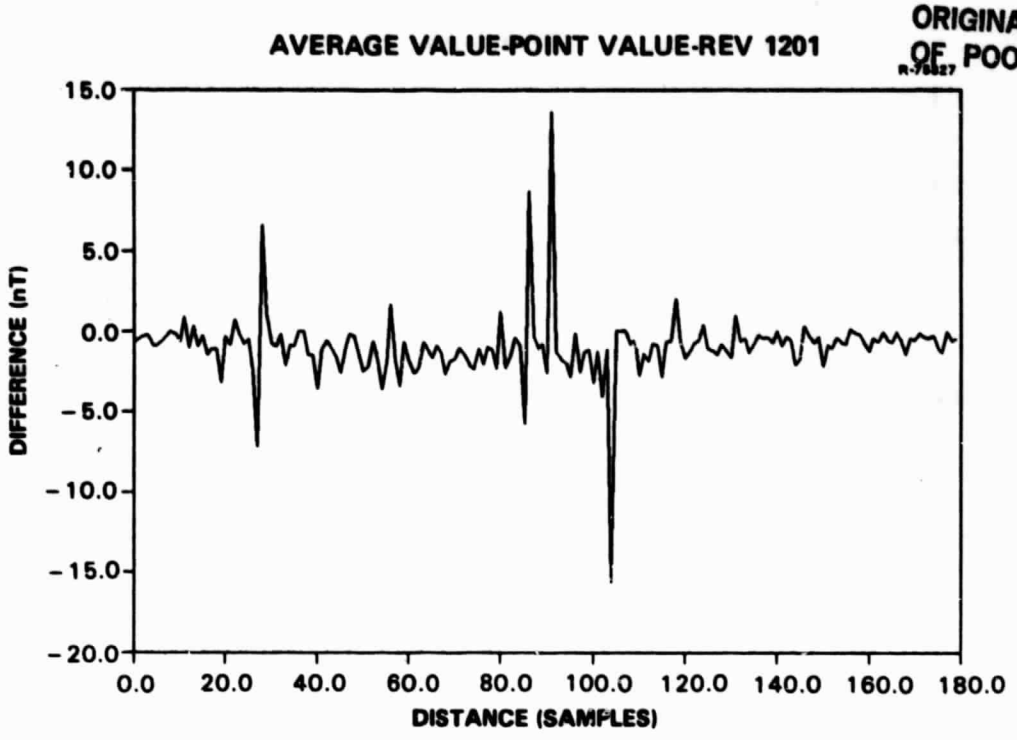

Figure 2-4 Field magnitude minus 80-point (36 km) running average

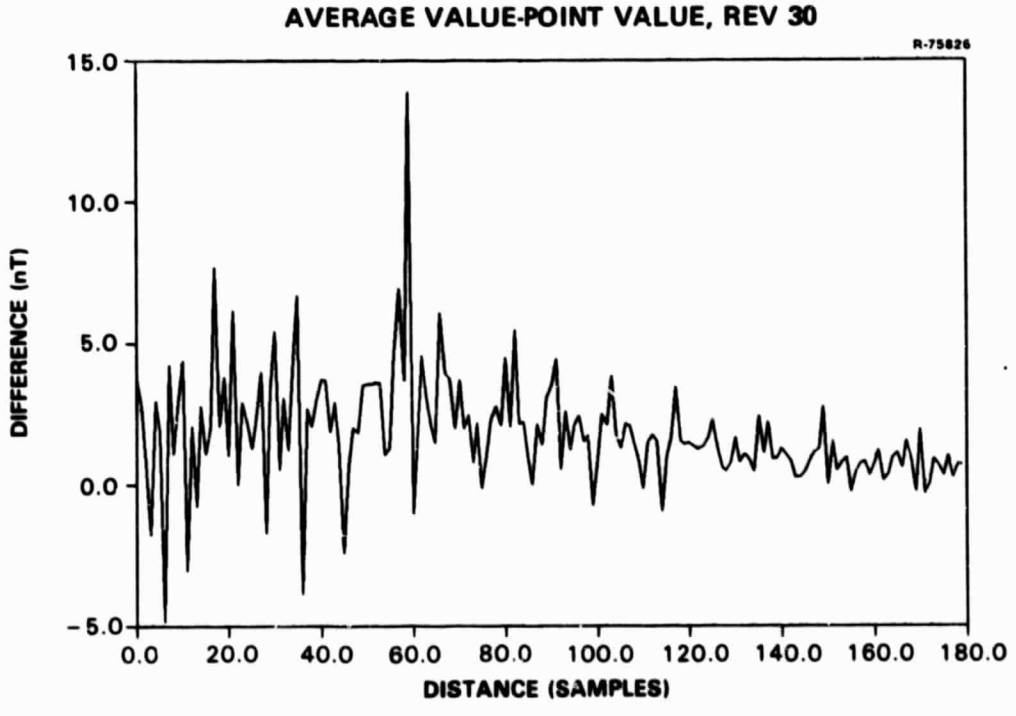

Figure 2-5 Z-component minus 80-point running average

The residuals are then assumed to be crustal magnetic anomalies plus external field effects. The external field effects are difficult to model, but the major effects are at longer wavelengths than crustal anomalies, and thus can be reduced by subtracting a ramp (or a low-order polynomial) from a pass of the residual data. This alters the spectrum of the data.

The effects on the data PSD of removing a mean, or mean and ramp, are illustrated in Fig. 2-6. This shows autoregressive spectrum estimates of order 5, for |B| anomaly data. Mean and ramp removal have no significant effect on the PSD for wavelengths shorter than 1050 km. Considering the confidence bounds (not shown in the figure) of these three PSDs, they are in agreement for wavelengths shorter than about 1900 km.

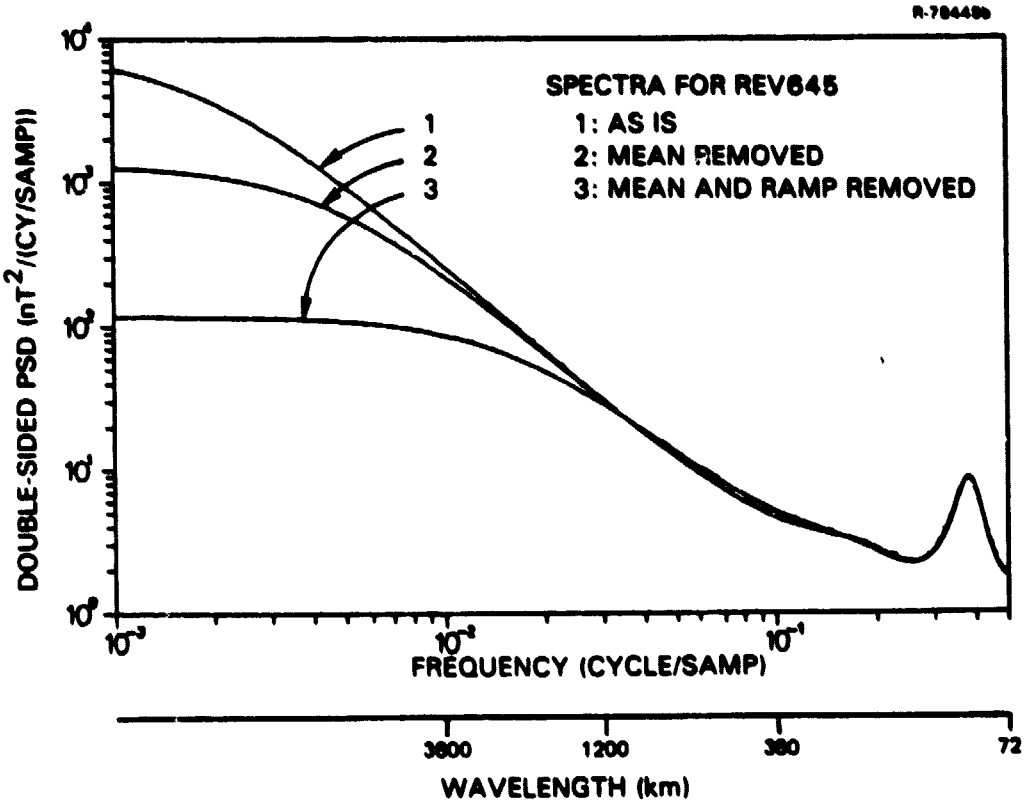

Figure 2-6 Curve 1 is an autoregressive PSD estimate for the data of Fig. 2-2 with spikes removed. Curve 2 is for the same data, but with the mean removed. Curve 3 is for the data with mean and ramp removed.

Further illustration of mean and ramp removal is shown in Fig. 2-7. The slope in the midsection of the spectra, and the noise floor are unchanged because mean and ramp removal are a form of high-pass filtering.

Subtracting the mean from the data removes any bias which may be due to instrument error or a uniform external field. Subtracting a ramp from the data is expected to remove primarily the effects of the major external current fields. However, mean and ramp removal will also take out any long-wavelength regional components, evident in single tracks, that may exist in the crustal field. Since the Magsat tracks are oriented nearly N-S, information in the E-W direction will be removed when the tracks are processed individually.

The conclusion is that, for tracks crossing the investigation region (and consisting of arcs of approximately 50 deg), the wavelength passband from 2800 km to 1050 km is modified by the removal of a mean or a mean and a ramp. The noise floor appears to be reached at wavelengths slightly shorter than 250 km. Thus, the band between 1050 km and 250 km contains information which may pertain to crustal geophysics and is unaltered by the removal of a mean or a mean and a ramp. The tradeoff invoked by mean or ramp removal involves decreasing or eliminating the effects of external fields at the expense of perturbing the data with wavelengths longer than about 1050 km in the TASC investigation area. With this analysis in mind, the linear trend removal procedure was followed (after correction of spikes and data gaps) for all tracks of "Quiet-Time" data crossing the study area. This was done prior to the production of anomaly maps, which are described in Chapter 4. However, before computing the anomaly maps, a power spectrum and resolution analysis was performed on along-track data. Those results are discussed in Chapter 3.

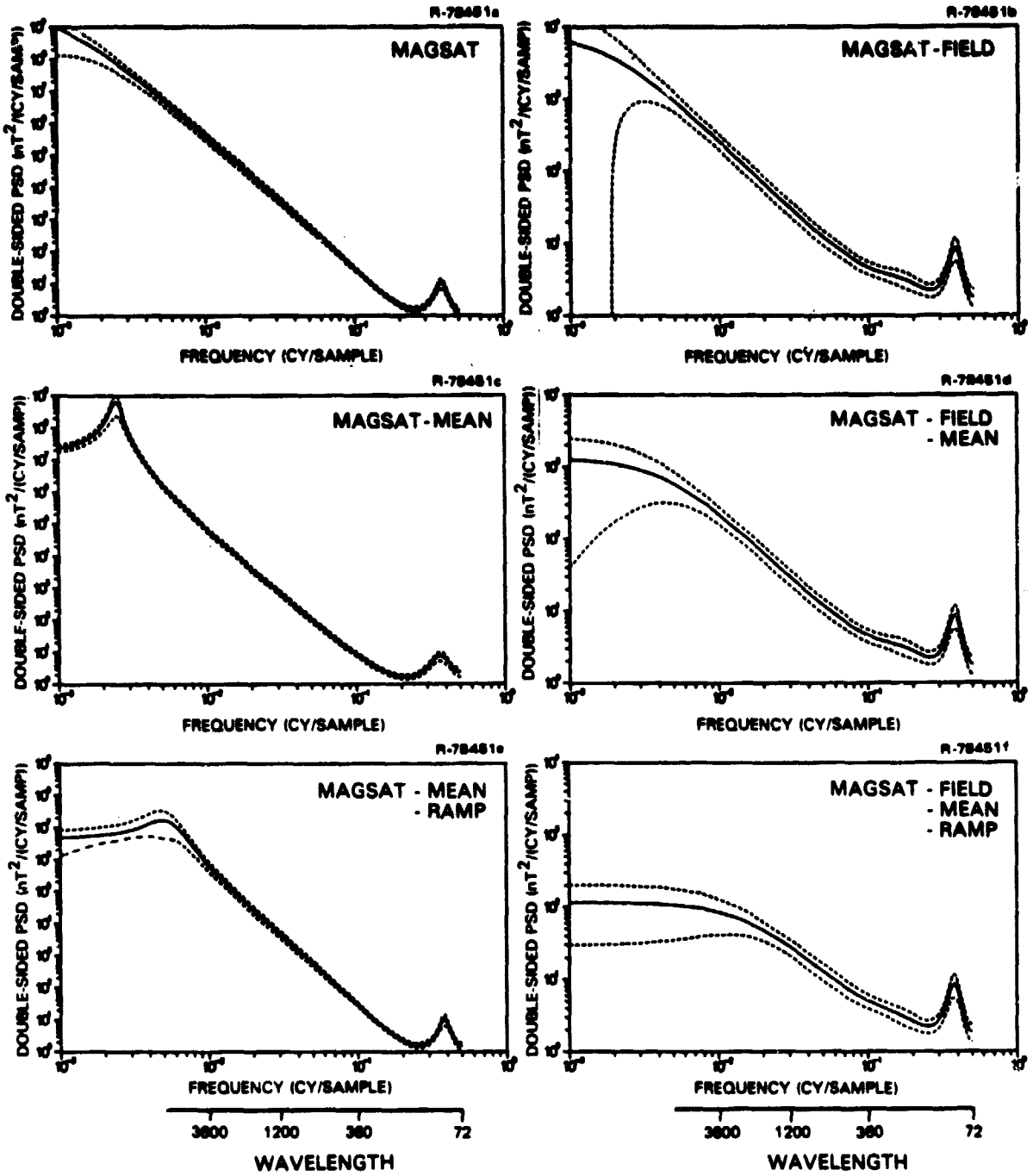

Figure 2-7 Spectral estimates for Rev 645, from Magsat data (on left) and Magsat minus field model (on right). Note the different vertical scales. Top to bottom rows are: unaltered data, mean removed, and mean and ramp removed. The dotted lines bound the 95% confidence level.

2.3 SUMMARY OF DATA PREPROCESSING

The following points summarize the data selection and preprocessing:

- Results presented in this report are based mainly on the Magsat Investigator-B data, limited geographically to the eastern Indian Ocean
- Scalar data (computed from the vector component data) were selected from data designated as "Quiet-Time" by NASA for production of magnetic anomaly maps
- Anomaly profiles were formed by subtracting values predicted by a degree and order 13 core field model, MGST(4/81-2)
- Spikes with amplitudes of up to about 20 nT occur in the anomaly profiles and were removed and replaced using a five-point moving window along the anomaly profiles
- Caution must be exercised when using the standard deviation of the 80-point running mean (provided on Investigator-B tapes), as this quantity mainly reflects the gradients of the main magnetic field. It does not reveal data spikes as clearly as the observed field quantity minus the 80-point running mean of that quantity
- A mean and ramp were removed from the arcs of data crossing the investigation region. This reduced anomaly power for wavelengths longer than about 1050 km, but does not affect shorter wavelengths.

3. ONE-DIMENSIONAL ALONG-TRACK ANALYSIS OF MAGNETIC ANOMALIES

3.1 CRUSTAL ANOMALY FEATURES ALONG TRACKS

The region of the eastern Indian Ocean covered by this investigation is shown in Fig. 2-1, which also shows several selected Magsat tracks. One objective of the first part of this investigation is to determine the characteristics of magnetic anomalies that might be associated with these features.

Figures 3-1 through 3-4 are anomaly profiles for Magsat Rev 45. Figure 3-1 is the residual total field magnitude, determined by subtracting the value predicted by the core-field model from the observed field magnitude computed from the three vector components. Figures 3-2 through 3-4 are the X, Y, and Z vector components. The locations of the major physiographic features are indicated on all of these plots. Some of the features in the anomaly profiles coincide with tectonic features. For example, a significant perturbation in the anomaly profiles is associated with the Broken Ridge and Diamantina Fracture Zone. This anomaly has an amplitude of about 10 nT and its form depends on the vector field component. Equivalent source modeling is necessary for further study of the origin and nature of this anomaly.

Figures 3-5 through 3-8 show the same type of anomaly profiles for Rev 685. Again, the locations of the major physiographic features are shown, and some of these are associated with features in the anomaly profiles. These profiles have

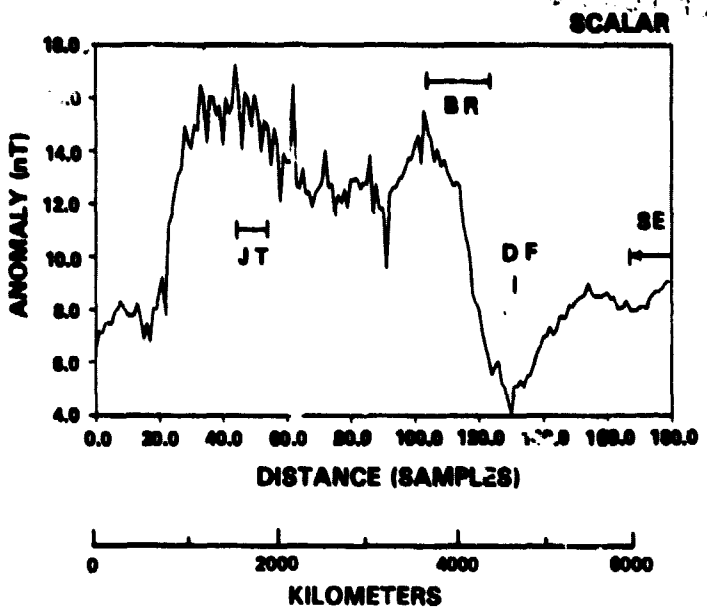

Figure 3-1 Anomaly profile for |B| from vector data of Rev 45. Average sample spacing is 35.3 km/ sample. Physiographic features indicated are: JT-Java Trench, BR-Broken Ridge, DF-Diamantina Fracture Zone, SE-Southeast Indian Ridge, NE-Ninetyeast Ridge

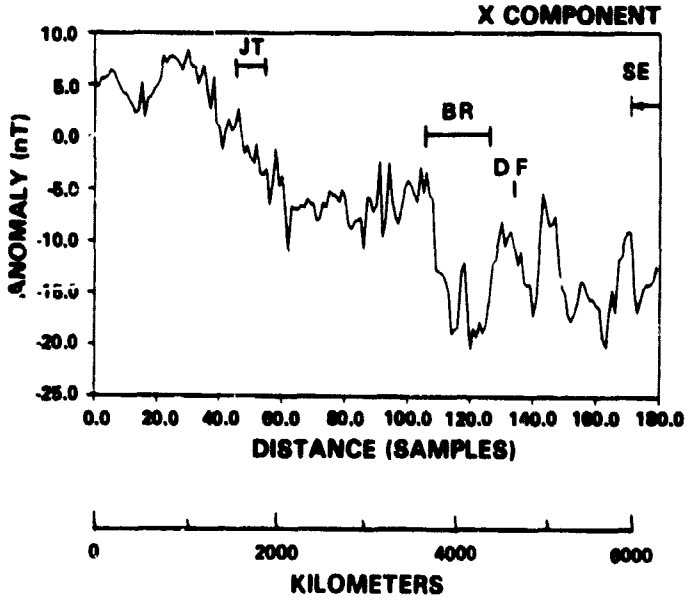

Figure 3-2 Anomaly profile for X-component, Rev 45. See Fig. 3-1 for key

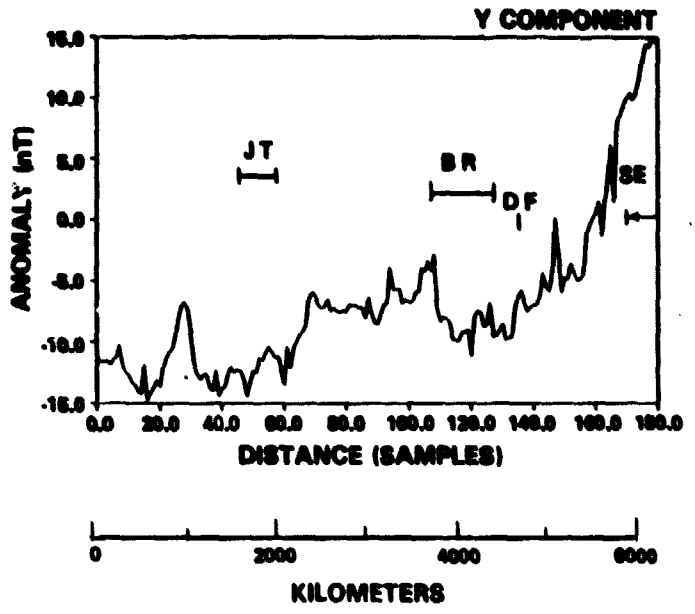

Figure 3-3 Anomaly profile for Y-component, Rev 45. See Fig. 3-1 for key

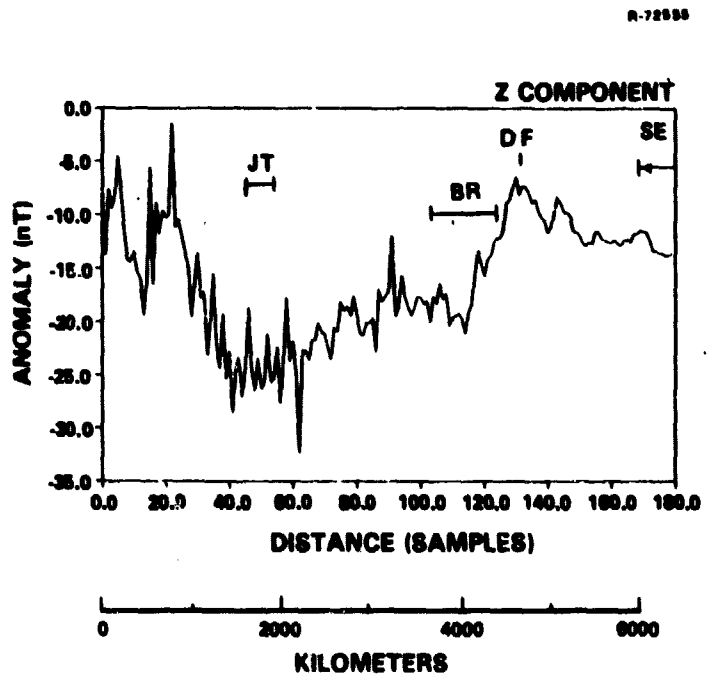

Figure 3-4 Anomaly profile for Z-component, Rev 45. See Fig. 3-1 for key

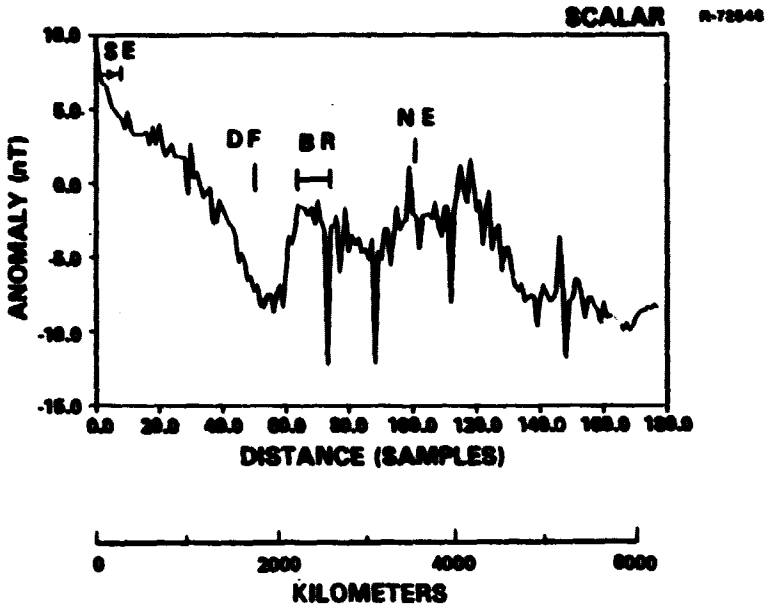

Figure 3-5 Anomaly profile for |B| from vector data of Rev 685. Average sample spacing is 36.3 km/ sample. See Fig. 3-1 for key.

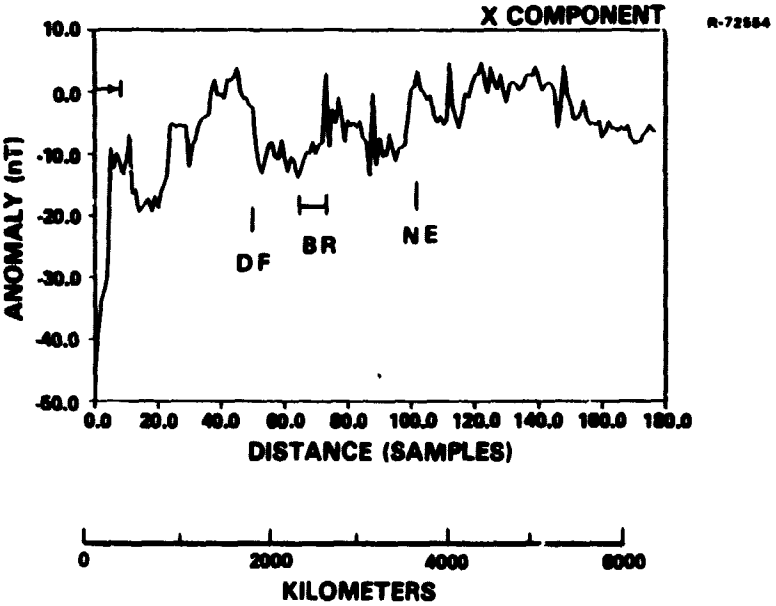

Figure 3-6 Anomaly profile for X-component, Rev 685. See Fig. 3-1 for key.

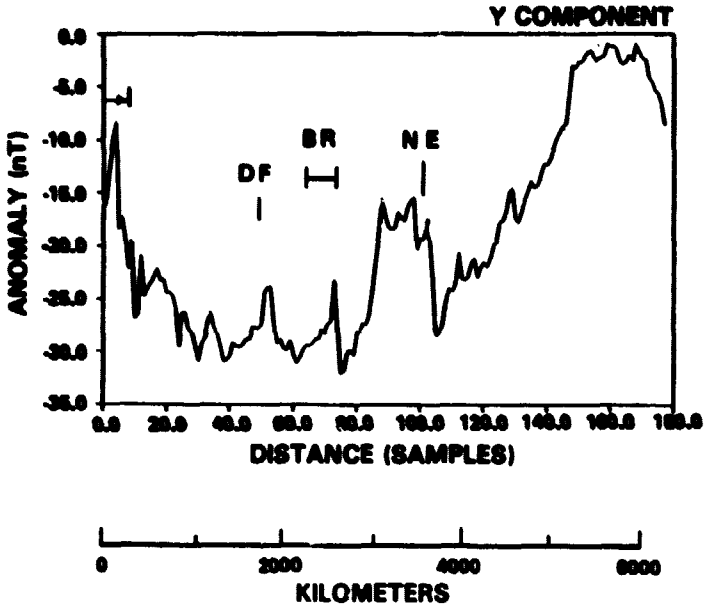

Figure 3-7 Anomaly profile for Y-component, Rev 685. See Fig. 3-1 for key.

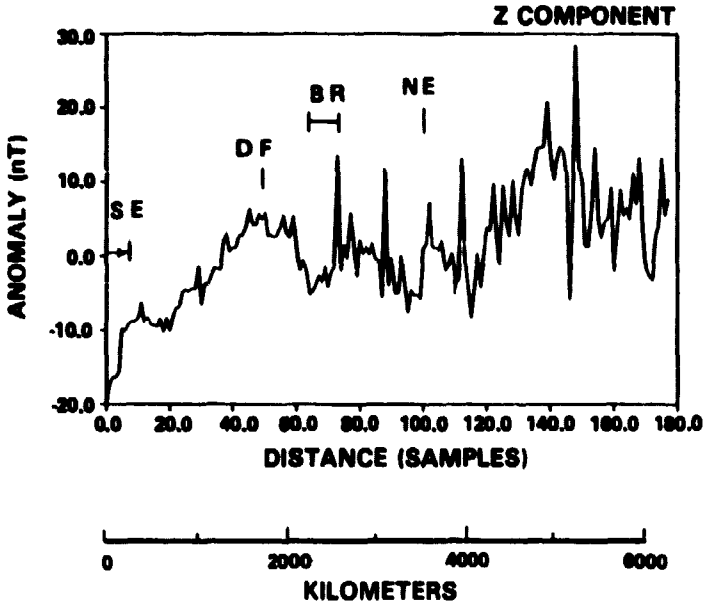

Figure 3-8 Anomaly profile for Z-component, Rev 695. See Fig. 3-1 for key.

more spikes than those for Rev 45, but the Broken Ridge-Diamantina Fracture Zone anomaly is still apparent, particularly in |B| (Fig. 3-5).

Figures 3-9 and 3-10 illustrate the repeatability of certain anomaly featues in Magsat data. Shown is the anomaly in |B| relative to the MGST(4/81-2) field model (Ref. 2). Although the scales on the plots are different, there is good qualitative agreement in the form of the major anomaly features. (Linear trends have not been removed from any of the anomaly profiles shown.) These and other magnitude profiles derived from the vector data, show consistency between "repeat" tracks, even though the anomaly profiles of the individual vector components appear to be more noisy and show less visual correlation with the corresponding component of other "repeat" tracks. This is because the individual components are more sensitive to satellite position and attitude than the magnitude values.

The most prominent anomaly feature in these tracks, associated with Broken Ridge and Diamantina Fracture Zone, has an amplitude of up to 10 nT. The anomaly features associated with the Java Trench and the Southeast Indian Ridge are not as consistent. It may be that anomalies associated with the latter features have longer wavelength components and thus do not show up as well against the background of the time-varying effects, which contribute long-wavelength trends to the profiles.

3.2 ALONG-TRACK DATA POWER SPECTRA

3.2.1 Examples of Magsat Data Spectra

Figure 3-11 is a typical Magsat data power spectrum estimate, from the anomaly profile shown in Fig. 3-1. This

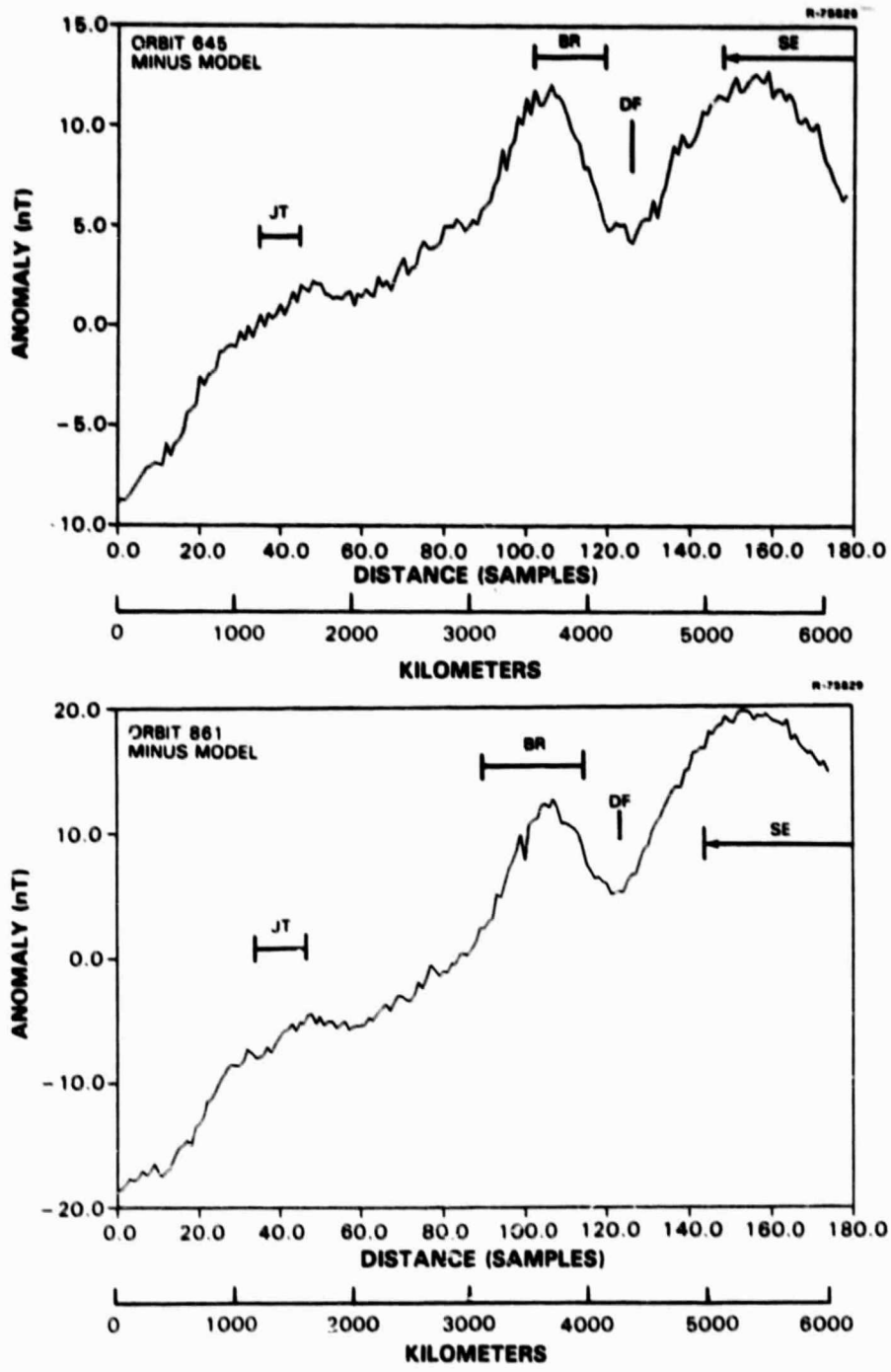

KEY: JT – JAVA TRENCH
BR – BROKEN RIDGE
DF – DIAMANTINA FRACTURE ZONE
SE – SOUTHEAST INDIAN RIDGE

Figure 3-9 Comparison of field magnitude anomaly for Revs 645 and 861

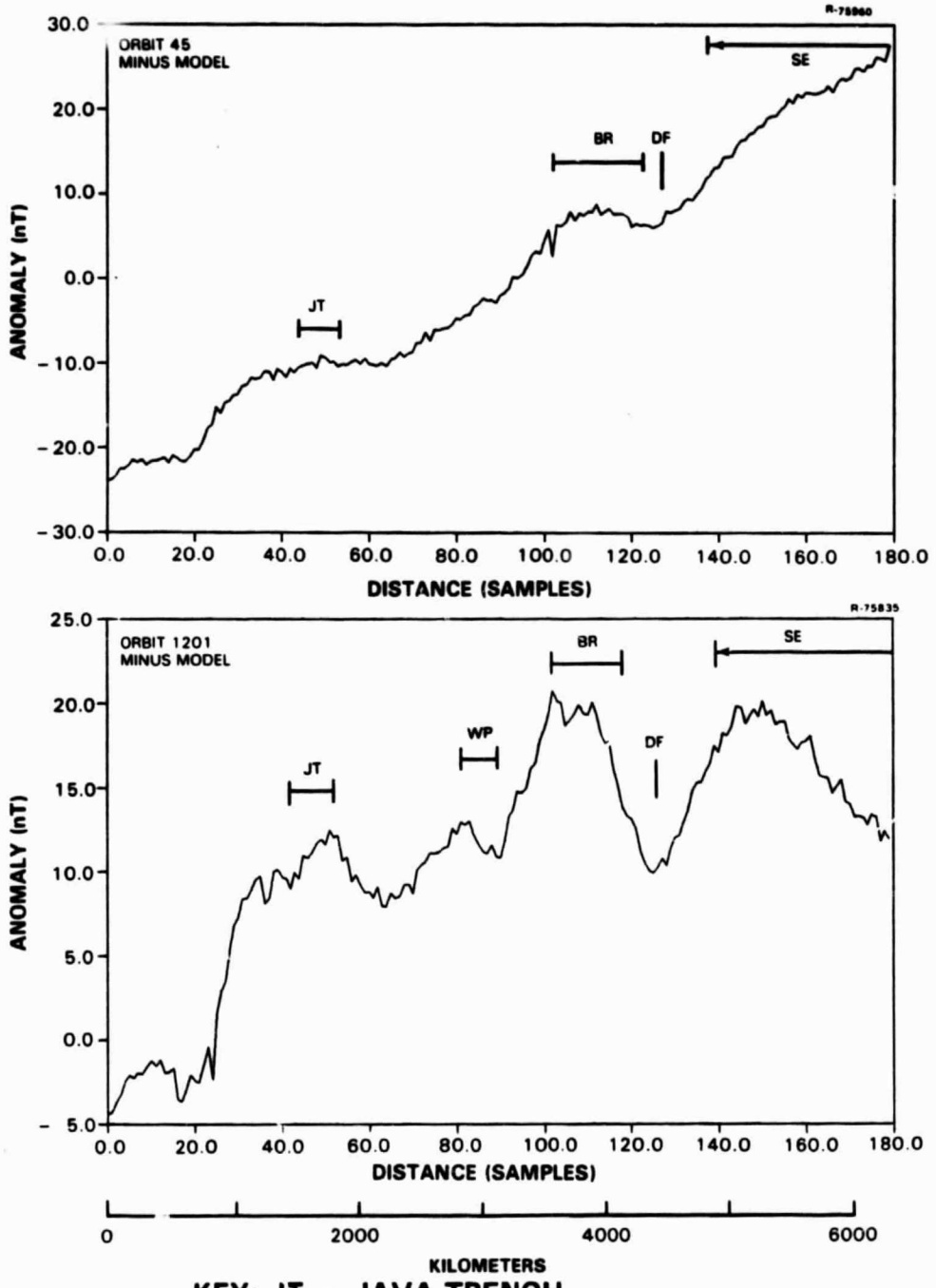

Figure 3-10 Comparison of |B| anomaly for Revs. 45 and 1201. Although the long wavelength components are significantly different between these two orbits, qualitatively, the anomaly features correlate well.

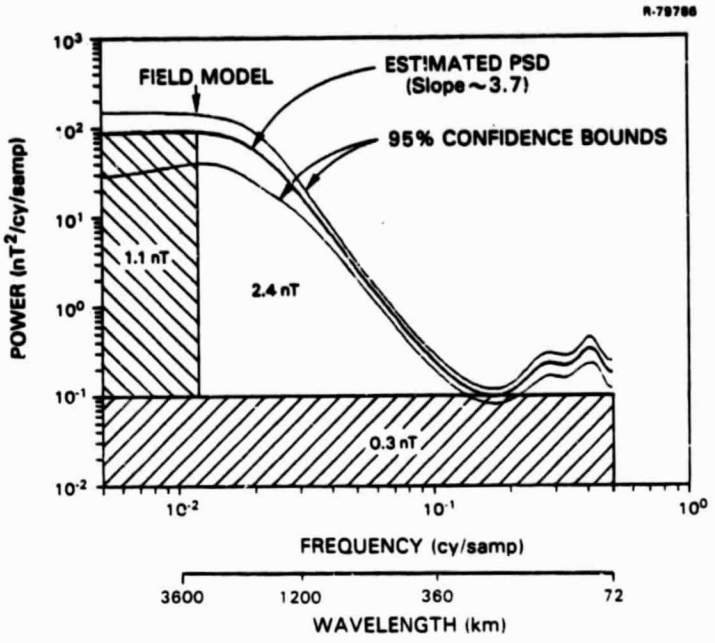

Figure 3-11 AR spectrum estimate with 95% confidence bounds for Rev 45, |B|. The total rms power is approximately 2.7 nT (including low frequencies not shown), with rms power in different sections as indicated. Dimensionless frequency is shown, sample spacing is ~35.3 km.

spectrum estimate was obtained by fitting autoregressive (AR) models to the anomaly time series. The 95% confidence bounds for this estimate were computed from the AR model parameters and the residuals. The optimum order for the AR model was chosen using an information criterion (Ref. 3). For the profiles analyzed, the optimum order ranges between two and seven.

The AR spectral estimates showed that the along-track Magsat spectrum may be divided into three portions. At low frequencies (wavelengths greater than 2900 km) the spectrum is flat, as the core-field model has removed most long-wavelength features. At intermediate frequencies, the spectra behave as a power law (f^{-b}), in this case (Fig. 3-11) with exponent, b,

of about 3.7. At high frequencies there is an apparent noise floor, beginning at about 10^{-1} sample^{-1} (corresponding to a wavelength of about 360 km). If it is assumed that this represents a component of white noise, then this component contains 0.3 nT rms. The interpretation is that this apparent noise floor represents instrument noise plus uncorrelated external field noise.

Table 3-1 lists the values for total rms power and noise level for spectra of all of the anomaly profiles of Figs. 3-1 through 3-8. The total rms power ranges between 9 and 56 nT with all but one of the spectra having less than 30 nT rms. The rms noise level is between 0.7 and 4 nT, with all except one case having less than 2.5 nT rms noise. For all of the spectra, the noise floor is reached at a wavelength of about 250 km. These results can be compared with the pre-Magsat mission specifications, i.e., a resolution limit of about 300 km for lithospheric anomalies and a noise level of about 3 nT for the vector magnetometer measurements. Since the Investigator-B data used for Fig. 3-11 were 80-point averages, the observed noise floor could be due to white noise with a level of 3 nT rms per original measurement, which when divided by $\sqrt{80}$ gives the 0.3 nT noise floor.

It should be emphasized that the spectra shown in this chapter are for one-dimensional analysis of the along-track power for individual tracks, and are appropriate for short wavelengths. For wavelengths much longer than about 5000 km, spherical harmonic analysis should be used. The next section discusses some of the relationships between spherical harmonic spectra, flat-earth two-dimensional spectra, and along-track spectra.

TABLE 3-1
RESULTS FROM SPECTRAL ANALYSES

REV #		FIELD COMPONENT (nT)			
		|B|	X	Y	Z
45	Total rms Power*	9.2	9.5	19.9	19.6
	rms Noise*	0.7	1.2	0.9	2.5
685	Total rms Power	10.2	56.3	29.4	11.1
	rms Noise	1.7	2.0	1.1	4.1

*The values given for |B| are the difference in magnitude between the observed field and the model field. These values are not equal to the magnitude of an anomaly vector formed from the X, Y, and Z anomaly components.

3.2.2 Models for Crustal Anomaly Spectra

The along-track power spectrum of Magsat data has been estimated and used as a tool to study the data quality and resolution capability. It would also be useful, for interpretation purposes, to know what these spectra are expected to look like for reasonable physical models of the earth's magnetic field. Analytic models for these spectra could allow study of the effects of instrument noise, external fields, and change in altitude. In this section, some preliminary results of model development are described. The purpose of this work was to develop a simple analytic model of along-track spectra that could both describe the data and be easily upward continued. A model that can be upward continued analytically can easily demonstrate the magnitude of the effects of satellite altitude on the observed power spectrum. This is important because features in the spectrum representing crustal magnetic

anomalies are attenuated rapidly with altitude and are obscured by noise when their power drops below a certain level. Further work is necessary to relate the parameters of this initial model to physical quantities such as magnetization of a crustal layer.

Upward continuation of a spherical harmonic power spectrum (The R_n defined by Lowes, 1974, Ref. 4) is accomplished by multiplication of the individual terms of degree n by the factor $(a/r)^{(2n+4)}$ (where a is the earth's radius and r is the radius of the observation point). For small values of altitude and for high degree, this spherical harmonic power spectrum,

$$R_n = (n+1) \sum_{m=0}^{n} [(g_n^m)^2 + (h_n^m)^2] \qquad (3\text{-}1)$$

asymptotically approaches a continuous flat-earth spectrum. For cases where the flat-earth approximation is valid ($r-a \ll a$, $n \gg 1$), a two-dimensional power spectrum, $\phi(\omega_x,\omega_y)$, is upward continued by multiplying the factor $\exp[-2h(\omega_x^2+\omega_y^2)^{1/2}]$. Thus,

$$\Phi(\omega_x,\omega_y,r) = \Phi(\omega_x,\omega_y)\cdot\exp(-2h\Omega) \qquad (3\text{-}2)$$

where $h = r-a$ is the height, and $\Omega^2 = \omega_x^2 + \omega_y^2$.

For along-track, or great-circle spectra, (such as would be observed along tracks of aeromagnetic or satellite data), upward continuation is not so straightforward. Formulae relating great-circle spectra to spherical harmonic spectra, and along-track spectra to two-dimensional isotropic spectra, have recently become available but have not been widely used. Thus, for example, the along-track (great-circle) aeromagnetic spectrum of Alldredge et al. (Ref. 5) was not

properly interpreted in many of the older papers which tried to relate these observations to global magnetic models. Recently, McLeod and Coleman (1980, Ref. 6) derived expressions for the relationships between great-circle and spherical harmonic spectra and applied these to model satellite observations.

To derive a simple model of Magsat along-track power spectra which permits upward continuation, the following assumptions are made: 1) the flat-earth approximation is valid for features in the wavelength range of interest, 2) the two-dimensional power spectrum is isotropic and has the form of an exponential. These assumptions allow the development of an analytic expression to describe the along-track power spectrum at any altitude. The second assumption is equivalent to stating that the two-dimensional power spectrum at any altitude may be described by the following function:

$$\Phi(\Omega) = c \exp(-b\Omega) \cdot \exp(-2\Omega h) \qquad (3\text{-}3)$$

where c and b are parameters, h is altitude, and Ω is radial frequency for the two-dimensional isotropic spectrum. This model is an "attenuated white noise" (AWN) type model since $\Phi(\Omega) = c$ at a depth of $h = -b/2$ (Ref. 7).

It can be shown that the along-track power spectrum, $S(\omega)$, corresponding to this two-dimensional power spectrum is the Abel Transform of Eq. 3-3 (Ref. 8). Thus,

$$S(\omega) = \frac{1}{\pi} \int_{\omega}^{\infty} \frac{\Omega\Phi(\Omega)}{\sqrt{\Omega^2 - \omega^2}} \, d\Omega \qquad (3\text{-}4)$$

The solution of this integral for the AWN model is:

$$S(\omega) = \frac{c}{\pi} \omega K_1 [\omega(b+2h)] \qquad (3\text{-}5)$$

where K_1 is the modified Bessel function (Ref. 9).

A choice of values for the parameters b and c was made by fitting Eq. 3-5 to an observed Magsat power spectrum at h = 300 km. (The modeling discussed here is being done for the spectrum of $|B|$.) The values obtained were $c = 1.0 \times 10^8$ and $b = 6.37 \times 10^{-1}$. With these parameter values for b and c, the function of Eq. 3-5 is plotted in Fig. 3-12 for altitude values of h = 150, 300, and 450 km. If it is assumed that the noise floor, representing white noise, is at the level of approximately 0.2 $(nT)^2/(cy/sample)$, then the resolution limit of satellite data would be approximately 160 km for h = 150, 350 km for h = 300 km, and 540 km for h = 500 km.

This model has certain simplifications: most notably the flat-earth approximation and isotropy of the two-dimensional power spectrum. However, the estimates of the resolution capability at different altitudes are reasonable. The formula of Eq. 3-4 is very similar to the formula of Eq. 27 of McLeod and Coleman (1980, Ref. 6), which is the asymptotic approximation of an expression describing the relationship between an average great-circle power spectrum and the spherical harmonic spectrum.

When plotted on a log-linear scale, the function (Eq. 3-5) has the form of a straight line with a slope = -2h, indicating that it is essentially exponential. This is the form of along-track spectra observed in aeromagnetic surveys and as modeled by Spector and Grant (1970, Ref. 10) for the purpose of determining depth to magnetic basement. The fact that our along-track spectrum estimates from Magsat data show power-law (straight lines on log-log plots), rather than exponential behavior, is discussed below.

R-80723

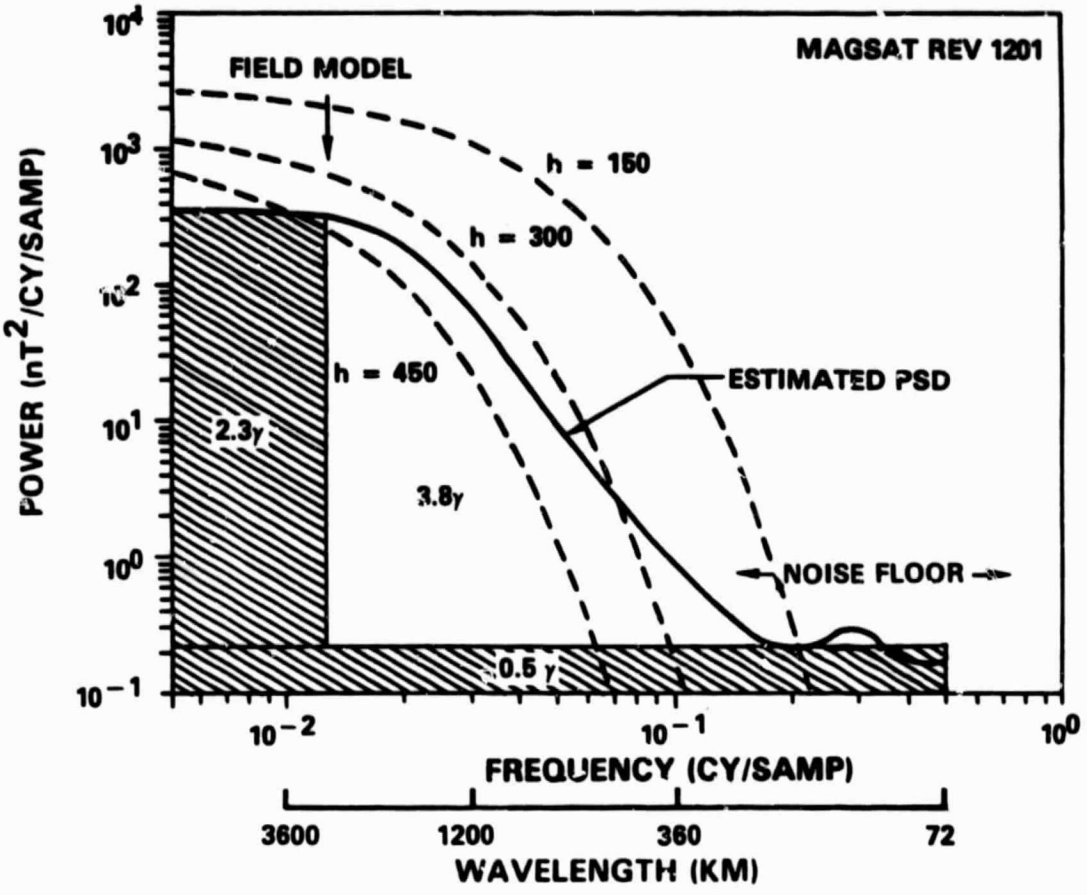

Figure 3-12 Observed Magsat spectrum for |B| of Rev 1201 compared with values given by the analytic model of Eq. 3-5. The effect of different heights h, is shown. (Rev 1201 was at h = 350 to 360 km during the pass over the investigation region.)

3.2.3 Verification of Spectrum Analysis Technique

Figure 3-12 compares an observed Magsat along-track power spectrum with curves predicted by a simple attenuated white noise (AWN) model of the magnetic anomaly field. The lack of agreement between the shape of these theoretical spectra and the estimated spectrum may be explained by the following possibilities:

- The spectrum estimation technique may not be sensitive enough to resolve the properties of the anomaly field from the relatively short time series of observed data
- Noise in the observations may distort the estimate of the spectrum of the crustal anomaly data
- The AWN model may not describe the actual behavior of the crustal anomaly field.

In order to investigate these possibilities, computational tests of the autoregressive spectrum estimation algorithm were performed using synthetic data. These synthetic time series are realizations of a process which has the AWN (modified Bessel function) along-track power spectrum.

The synthetic time series were formed by computing a realization of the process in the frequency domain and then using the FFT to produce a time series. The PSD of the desired discrete-time zero-mean random process is $S_{xx}(F)$, where F is frequency in cycles/sample. The goal is to construct a time series $\{y_k, k = 0,1.2,...n-1\}$ that is a realization of this process. The first step is to construct the periodic complex sequence u_j, $j = 0,1,2,...N-1$, with period $N>>n$, given by:

$$u_j = (a_j + ib_j)\sqrt{N\, S_{xx}(F)} \qquad (3\text{-}6)$$

where the frequency $F = j/N$ and $\{a_j\}$ and $\{b_j\}$ are independent realizations of zero-mean white-noise processes, each with unit variance. Then the FFT of the sequence u_j is a complex periodic sequence, Z_k, with period $N>>n$ such that

$$y'_k = Re[Z_k(N)], \quad k = 0,1,2,3,...,n-1 \qquad (3\text{-}7)$$

and

$$y''_k = \mathrm{Im}[Z_k(N)], \quad k = 0,1,2,3,\ldots,n-1 \qquad (3\text{-}8)$$

are two independent realizations of a process that approaches the desired process y_k as $N/n \to \infty$.

To construct the realizations appropriate for the Magsat problem illustrated in Fig. 3-12, N was 8192 and n was 180 samples. The spectrum $S_{xx}(F)$ was given by

$$S_{xx}(F) = CFK_1(2\pi F(b+2h)) \qquad (3\text{-}9)$$

where K_1 is the modified Bessel function, F is frequency in cycles/sample, the parameter $C = 5.556\times10^{6}$ nT^2/cycle/sample, the parameter $b = 1.764\times10^{-2}$ samples, and h = 8.333 samples (h represents a height of 300 km, expressed in terms of the typical distance between samples which is 36 km). The computed realizations were then comparable to the Magsat data provided on the Investigator-B tapes.

A series of numerical experiments were conducted, using synthetic time series of varying length as inputs to the AR spectrum estimator. Figure 3-13 is the result of one of these computations. There is excellent agreement between the spectrum estimated by the autoregressive technique (using 360 samples) and the original theoretical (AWN) spectrum. These and other computations verify that the TASC autoregressive spectrum estimation technique is capable of resolving an exponential-type spectrum in the absence of noise, even when as few as 180 samples are used.

When white noise is added to the synthetic times series (to represent the measurement errors of the Magsat magnetometer), the AR spectrum estimation requires more samples to obtain an

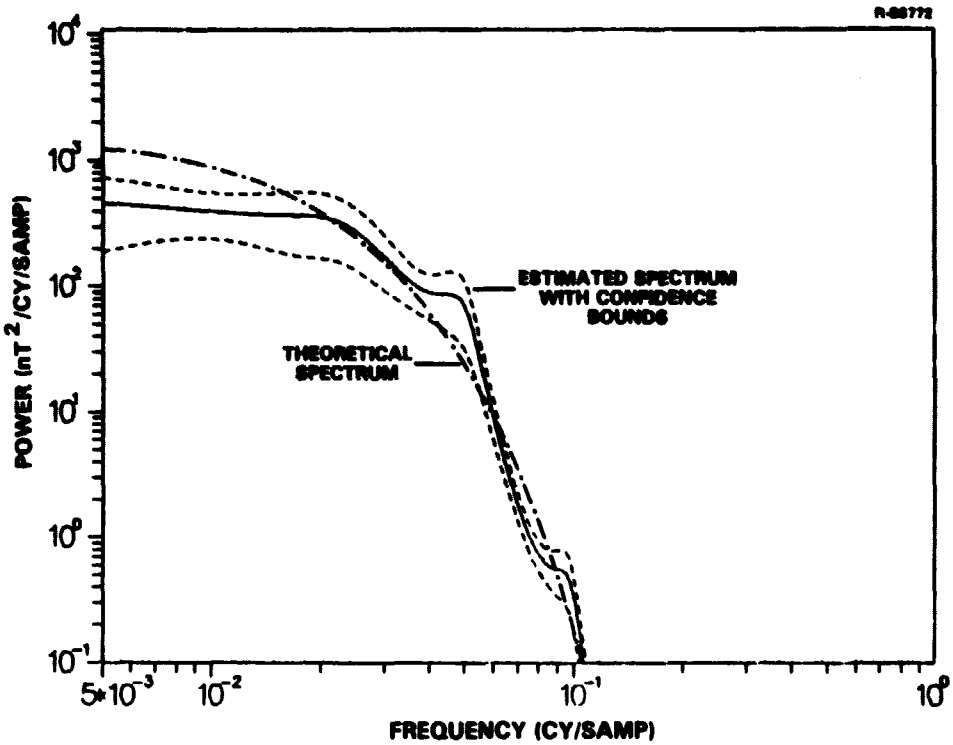

Figure 3-13 Comparison of theoretical PSD (dash-dot) curve) and PSD estimated from synthetic time series (360 samples)

accurate estimate. As more and more white noise is added, the spectrum estimate using only 180 samples becomes biased in that it has a less-steep slope in the frequency range between 0.01 and 0.1 cycles/sample. However, when white noise with σ = 0.5 nT (Fig. 3-12) is added, the spectrum estimate using only 180 samples is still able to resolve the steepening roll-off of the PSD at frequencies lower than 0.1. This result is shown in Fig. 3-14.

Since the accuracy of the spectrum estimation technique and the effects of noise have been established, it is concluded that: the spectrum of Magsat data is not modeled well by an AWN contribution plus white noise. While the AWN model for the crustal anomaly field cannot be ruled out, Magsat along-track data may contain some colored noise which reduces the rate of

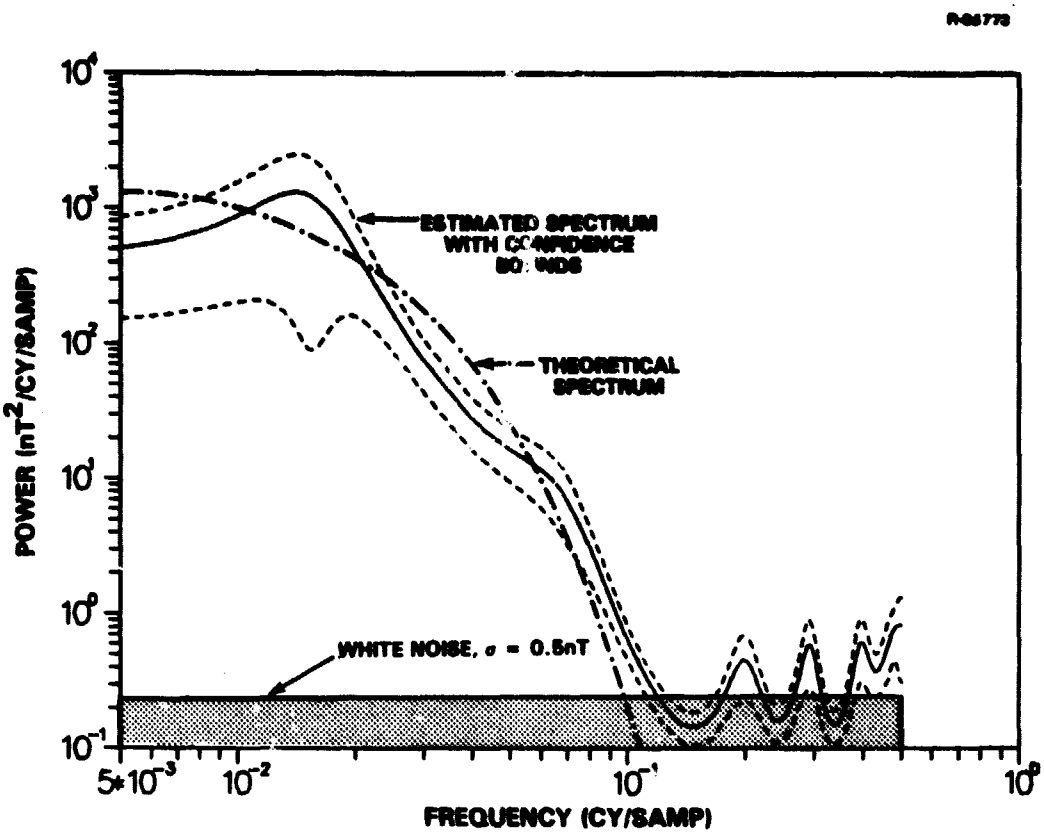

Figure 3-14 Results of spectrum estimation test using synthetic data plus white noise with σ = 0.5 nT

roll-off of the estimated spectrum. The colored noise may be due to variations in the external field, and thus would be uncorrelated between adjacent Magsat tracks. The presence of this colored noise might account for the fact that spectral coherence between nearly coincident Magsat tracks is not significant for wavelengths less than 700 km, even though the noise floor of individual Magsat spectra is not reached until wavelengths as short as about 300 km (see Section 3.3, and Ref. 11).

The following points summarize the results of the tests that verified the technique of spectrum analysis of along-track Magsat data:

- **The TASC AR spectrum estimation technique is capable of giving correct spectrum estimates from relatively short time series of observations such as the Magsat data**

- **The spectrum estimates obtained from Magsat crustal anomaly profiles are not consistent with a model in which the data spectrum consists only of an AWN component (from crustal anomalies) plus white noise (from the sensor)**

- **The spectrum estimates and spectral coherence computations from Magsat data indicate that these data may contain a noise contribution from the external field and that this contribution may have more power than the crustal anomaly field for wavelengths less than about 700 km.**

These conclusions have important implications relative to the production and interpretation of crustal magnetic anomaly maps from Magsat data. More work is necessary to ensure that the time-varying effects of the external field do not contaminate these maps.

3.3 SPECTRAL COHERENCE AND RESOLUTION

Magsat tracks which are geographically separated by less than about 100 km along the entire track segment are considered repeat tracks. Some of these are shown in the map of Fig. 2-1. This separation, and the altitude variation, are both small compared to the geophysically significant correlation distances in major crustal magnetic anomalies. Within the usable wavelength passband (1050 to 250 km) described in Section 2.2, computations were performed to find where the data are repeatable from track to track (high coherence), and where they are not (low coherence). The shortest wavelength

to which data are repeatable represents a resolution limit for the data. This limit must be taken into account when constructing two-dimensional maps from the data.

In this section, the concept of repeatability is quantified and illustrated in the frequency domain by computations of spectral coherence between nearly repeating tracks. These computations have defined two bands of differing behavior within the usable data passband (1050 to 250 km). A high coherence passband (1050 to 700 km) defines the region where the data are repeatable and the spectrum of the data can be considered to contain geophysically significant information. A low coherence passband (700 to 250 km) defines that part of the data which is not repeatable from track to track, but which may still contain useful data along single tracks. The low coherence in this passband is partly due to track separation and partly to colored (f^{-n}) noise, possibly caused by the time-varying external field.

A quantitative measure of repeatability is provided by the spectral coherence function (Ref. 12) which is the squared correlation coefficient of the data along the tracks at each frequency (or wavelength) in the spectrum. Spectral coherence, $\rho(\omega)$, is defined as follows:

$$\rho(\omega) = \frac{|S_{xy}(\omega)|^2}{S_{xx}(\omega)S_{yy}(\omega)} \qquad (3\text{-}10)$$

where, for the two tracks x(t) and y(t), S_{xx} and S_{yy} are the corresponding auto-spectra and S_{xy} is the cross-spectrum. Autoregressive methods of spectrum estimation are discussed in Ref. 13.

The coherence between pairs of repeat tracks is reduced from the maximum value of 1 by non-repeating errors or noise in the individual measurements. The observed Magsat data is composed of the signal (considered here to be crustal anomalies) and noise (e.g., instrument noise, orbit errors, time-varying external fields). The noise is the major contributor to the non-repeatable portions of the spectra, more significant than effects due to the fact that the pairs of tracks do not perfectly match in altitude and position.

An autoregressive spectral estimation algorithm was applied to the Indian Ocean sections of Rev 645 and Rev 861. These two tracks are separated by 49 to 92 km in surface distance, and by 70 to 80 km in altitude. This spectral estimation algorithm differs from that used in Section 3.1 in that it uses information from both tracks to estimate the spectra of either track. Thus, where the two tracks are coherent, the two-channel spectral estimate is better (as it operates on more data). This algorithm then estimates the coherence between the two tracks (Eq. 3-10), which is a measure of how well one track can be predicted from the other. The result is shown in Fig. 3-15. The anomaly profiles are visually comparable after linear trends have been removed.

The spectral structure in Fig. 3-15 is more detailed in appearance than those than shown and discussed in Section 3.2.1. The spectral estimation algorithm chose order 10 as the best fit here, versus order 5 chosen previously. This may be partially due to the increase of the available data (two tracks are used simultaneously). A spectral peak at about 1700 km is clearly evident here, and was not seen with the order 5 model. The cause of this peak is a nearly periodic structure of the data, as may be seen in the time series of Fig. 3-15.

ORIGINAL PAGE IS
OF POOR QUALITY

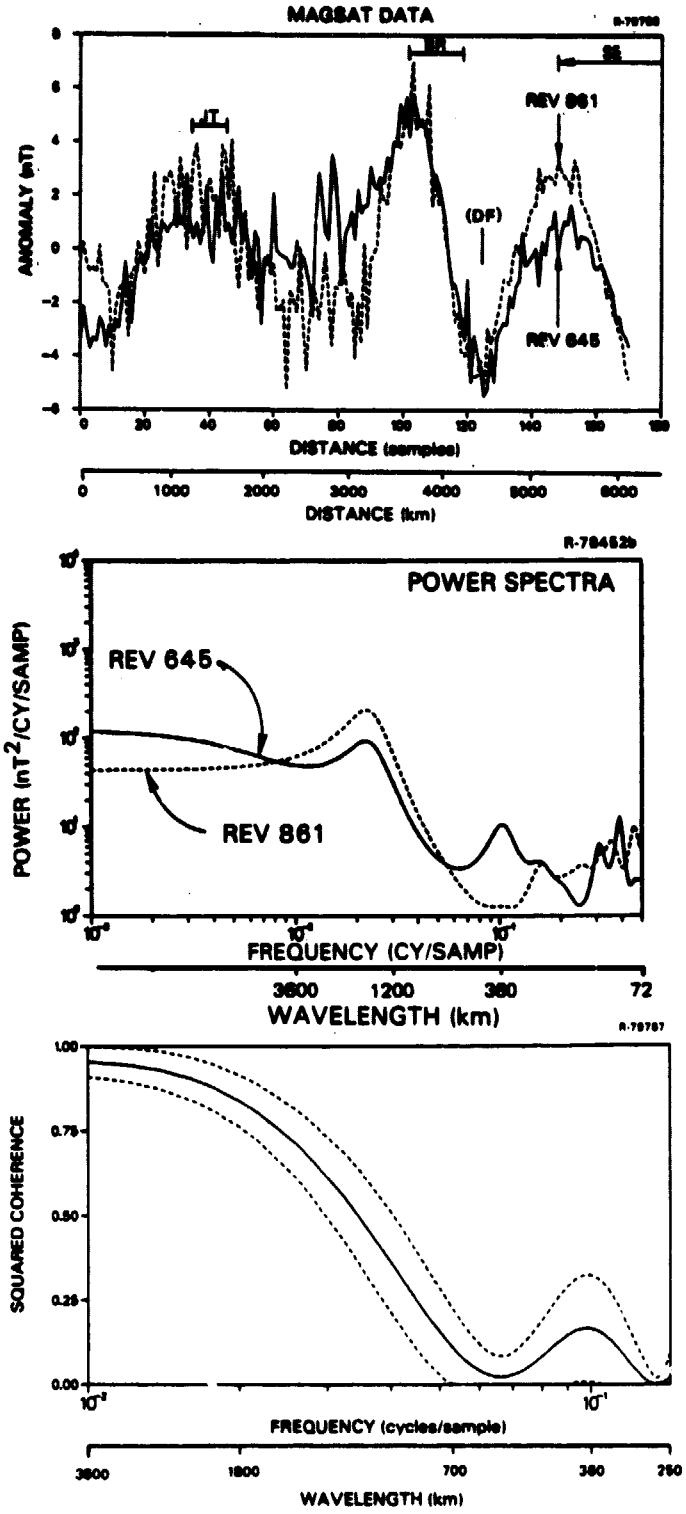

Figure 3-15 Top: two repeat tracks, Rev 645 (solid line) and Rev 861 (dashed line), linear trends removed. Middle: the estimated spectra, where the two-channel auto-regressive spectral estimation algorithm chose order 10 for the best fit to the data. Bottom: spectral coherence between the two tracks.

Figure 3-15 also shows the squared coherence between the two repeat tracks. The dashed curves are 95% confidence bounds, which reach zero coherence at a wavelength of about 700 km. This means that wavelengths shorter than about 700 km are not repeatable from track to track. Results from other coherence computations using other repeat track pairs show that coherence becomes either insignificant, or less than 0.5, at wavelengths between 800 and 700 km.

The conclusion then, is that wavelengths longer than about 700 km have significant coherence, while wavelengths shorter than 700 km are not coherent. Figure 3-16 (from Ref. 11) summarizes these observations about the usable information content of each wavelength band.

The low coherence in the band between 700 and 250 km does not mean that geophysical information cannot be obtained in this band. It could be due to variations in altitude and geographic position of the repeat tracks, or, the low coherence in this band could be due to external field noise, which would vary from track to track. The properties of this band must be investigated further with gridded data and by comparison with gravity data.

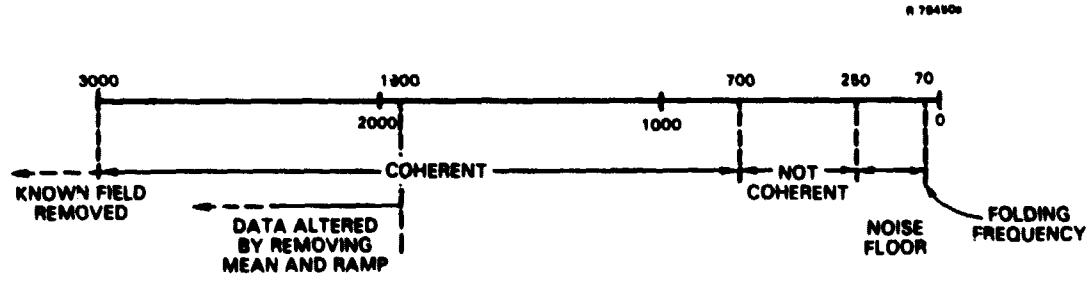

Figure 3-16 Properties of different regions of the Magsat along-track power spectrum, as determined from spectrum analysis and coherence studies. Numbers indicate wavelengths in km.

The results of this and the previous section suggest that low-pass filtering and decimation of Magsat data into sampling intervals substantially longer than the 80-sample averages now available on the Investigator tapes would not degrade the analysis of crustal magnetic anomalies. Low-pass filtering and decimation over as many as 200 to 300 samples could result in more cost-effective data analysis as it would only delete incoherent noise.

3.4 SUMMARY OF ALONG-TRACK ANALYSIS

The following points summarize the analysis of individual tracks of Magsat data crossing the eastern Indian Ocean:

- Anomaly profiles of the field magnitude |B| show better visual correlation with tectonic features than anomaly profiles of the X, Y, or Z components
- The most consistent anomaly feature observable on profiles is associated with Broken Ridge, and has an amplitude of up to 10 nT. Other physiographic features such as Diamantina Fracture Zone, Ninety-east Ridge, Southeast Indian Ridge, and Java Trench are associated with smaller visible features in the anomaly profiles
- PSD estimates derived from anomaly profiles show that the spectra have a power law (f^{-b}) behavior and reach a noise floor at short wavelengths between 360 and 250 km
- Numerical experiments with synthetic data have verified the technique of spectrum analysis and have showed that Magsat along-track anomaly profile spectra are not simply described by an AWN crustal field (Section 3.2.3) plus white noise

- Computations of the spectral coherence between pairs of closely-spaced Magsat tracks show that wavelengths shorter than 700 km are not highly coherent, while longer wavelengths are more repeatable from track to track

- Analysis of power spectra and spectral coherence indicate that the Magsat data sampling interval could be lengthened from about 36 km to about 125 km. This would reduce the data handling requirements.

4. TWO DIMENSIONAL ANALYSIS OF MAGNETIC ANOMALIES

This chapter builds upon the one-dimensional analysis of Chapter 3 and describes the construction of the two-dimensional magnetic anomaly maps from Magsat data. The technique used is equivalent source modeling which was developed and applied to anomaly map production by Mayhew and others (Refs. 14, 15, 16). This involves using a grid of equivalent source magnetic dipoles, and an important question concerns the optimum grid spacing for these model dipoles. The resolution capability analysis provides guidance in this choice.

Section 4.1 describes a survey simulation which represents how well one could expect satellite magnetic anomaly surveys to agree with high-altitude aeromagnetic surveys. It does not take into account some of the inaccuracies that might be introduced by the equivalent source technique, but it is presented here for reference, as it shows the effects of changes in the satellite altitude. This type of simulation should be used in the planning of future satellite magnetometer missions.

Since the TASC investigation used the NASA-supplied software (ESMAP) to perform the equivalent source inversion and produce anomaly maps, this software was first tested. These tests, described in Section 4.2, confirmed that ESMAP was working correctly when installed at TASC.

The remainder of Chapter 4 (Sections 4.3, 4.4, and 4.5) describe the results of equivalent source inversions:

maps of magnetic anomaly for the Broken Ridge Area, for the entire investigation area, and maps of relative crustal magnetization and susceptibility.

4.1 MAGSAT SURVEY SIMULATION AND MAP RESOLUTION

Based on experience with analysis of gravity survey data, TASC developed a survey simulation to estimate the accuracy of various satellite survey configurations for extracting the crustal magnetic anomaly field. The analysis is performed in the two-dimensional spatial frequency domain, taking into account the geometry of the survey (e.g., orbit inclination, altitude) and the power spectra of: external field noise, instrument noise, and the crustal anomaly field to be derived from the noisy observations. In addition to the effects of the external field and instrument noise, the analysis takes into account the errors caused by aliasing and the pattern of track coverage. However, in the current software, a constant altitude (circular orbit) has been assumed.

The simulation requires spectral models for the crustal anomaly field, the external field noise, and the instrument noise. For the results shown here, the instrument noise was modeled as white noise with an rms of 0.3 nT. The external noise power spectrum was modeled according to a formula based on observatory data (Ref. 17):

$$P_z = (3.68 \times 10^{-5}/f^2) \exp(-2.25f) \qquad (4\text{-}1)$$

The crustal anomaly field was modeled as white noise at the earth's surface: 0.082 $(nT)^2$/cycle/rev) (Ref. 18). This modeling pertains to the vertical component of the field.

Table 4-1 illustrates the results of several runs of the survey simulation program. Results are shown for several different satellite altitudes, assuming a constant altitude and a track separation of 1/2 degree at the equator. In this case, the analysis is concerned with wavelengths between 3000 km and a variable short wavelength cutoff (λ_s), which might be chosen for low-pass filtering of the data to remove short wavelength noise. The results of the different runs are expressed in terms of the rms residual power that would remain within the indicated wavelength band after the survey. The residual power represents survey errors plus noise and is the magnitude of the error made if it were assumed that the output of the survey represented the crustal anomaly field.

TABLE 4-1

RESULTS OF SURVEY SIMULATION
RMS RESIDUAL VERTICAL FIELD COMPONENT (nT) IN THE BAND 3000 km $\geq \lambda_{EAST}, \lambda_{NORTH} \geq \lambda_s$

λ_s (km)	RAW FIELD	HIGH ORBIT (600 km)	INTERMEDIATE ORBIT (450 km)	INTERMEDIATE ORBIT (200 km)	LOW ORBIT (160 km)
100	221.4	218.4	216.1	193.3	176.1
300	75.9	66.8	58.6	6.1	2.4
500	45.5	28.0	13.8	0.6	0.3
700	32.2	8.3	2.2	0.2	0.1

Since the analysis includes the effects of upward or downward continuation, the residuals may be computed at any altitude. For this table, rather than computing the residuals at satellite altitude, they are all expressed at a common altitude of 1000 meters. This allows comparison of results in terms of a high altitude aeromagnetic survey, such as Project

Magnet. The different columns of Table 4-1 quantify how the residuals decrease with decreasing satellite altitude. The rows illustrate the change in both the residuals and the raw field as the short wavelength cutoff is changed. For example, if wavelengths between 3000 and 700 km are considered, then the satellite survey at 600 km altitude would be able to map the anomaly field to within 8.3 nT (from a total raw field power of 32.2 nT) at 1000 m. If wavelengths between 3000 km and 300 km are considered, then the residual is 67 nT (from a total raw field power of 76 nT). However, if the satellite altitude is decreased to 160 km, the errors would be much smaller. This is an example of how a survey simulation can be used to plan and evaluate different proposed mission configurations and data reduction techniques.

4.2 EQUIVALENT SOURCE INVERSION

The NASA-supplied Investigator-B tapes ("quiet-time" Magsat data for the TASC investigation area) were previously found to contain bad data points which were categorized as follows: 1) known missing data values (flagged with a 99999.0) and 2) isolated data spikes with values greater than about 15 nT. There are also points with incorrect values for latitude, longitude, or altitude. These points and all tracks consisting of less than 20 points were deleted from the investigation data set. A linear trend was removed from each track of data to reduce the effects of external fields. Since we believe that the data sampling rate can be lowered (Section 3.3), the remaining edited and de-trended data was averaged over five consecutive points and stored on a new and condensed version of the Investigator-B tapes. This averaging increased the sampling interval from 36 to 180 km.

The goals of this research include producing a magnetic anomaly map and forming a joint interpretation of magnetic and gravity anomaly data. To accomplish these tasks, it is necessary to reduce the Magsat data to a regular grid at a constant altitude and to infer the associated crustal magnetization. The computer program ESMAP obtained from NASA, is particularly well suited for these purposes. ESMAP uses a least-squares fitting algorithm to adjust a magnetization parameter (dipole moment per unit volume) of individual dipoles arranged in a grid, such that the resulting field fits the input satellite scalar data. The dipoles are located in the crust and oriented along the Earth's main magnetic field to simulate induced magnetization. Once the magnetization parameters have been determined for the equivalent source dipoles, a gridded magnetic anomaly map can be computed from those dipoles. The resulting anomaly map can be reduced-to-the-pole by reorienting the dipoles to a vertical position.

Since ESMAP is a complex software package, several tests were run to check for internal consistency, and an attempt at independent verification of the computed field points was made. The purpose of the testing was to 1) check that ESMAP could reproduce a model anomaly field (internal consistency), and 2) convert the magnetization parameter computed for the model dipoles into an estimate for magnetic susceptibility. Given the magnetization parameter of a single dipole, a computation independent of ESMAP for the resulting field can be made and compared with ESMAP computations.

Three tests were run, leading to a preliminary equivalent dipole source model and estimated anomaly map for the TASC investigation area. Test 1 fit a matrix of 25 dipoles in the investigation area to a small number of data tracks and

computed an anomaly field. Test 2 fit a single, centered dipole to the resulting field from Test 1 and computed an anomaly field and a reduced-to-pole anomaly field. Finally, Test 3 fit a matrix of 25 dipoles to the anomaly field from Test 2. These tests confirmed the internal consistency of the ESMAP algorithm. Each test (Sections 4.2.1 - 4.2.3) and the preliminary model of the field (Section 4.3) covered the entire 50 by 50 degree area and produced anomaly maps on a 1 by 1 degree scale at 350 km altitude. All of these magnetic anomaly maps have inaccuracies near the edges (a 12.5 degree border) as described by Horner (Ref. 15).

4.2.1 Test 1: Initial Software Test

Thirty tracks (3621 points) of data were processed to fit 25 dipoles (10 degree spacing). The results are shown in Fig. 4-1a. The first estimate for the anomaly field compares roughly with the published two-degree Magsat map regarding the location and amplitude of the major feature located near the Broken Ridge. However, the broad spacing of the dipole locations leads to a "ripple" effect visible in the anomaly map and clearly indicates the need for a denser dipole grid in the further stages of this investigation.

4.2.2 Test 2: Single Dipole Fit and Reduction to Pole

The gridded anomaly map resulting from Test 1 was used as input data for this test. A single, centered dipole was fit to the 1601 input data points. The purpose of this test was to generate a single dipole field. It was simpler to let ESMAP fit a single dipole field to an arbitrary field, than to generate a single dipole field analytically. Since only one dipole was fit, the magnetization has a very high

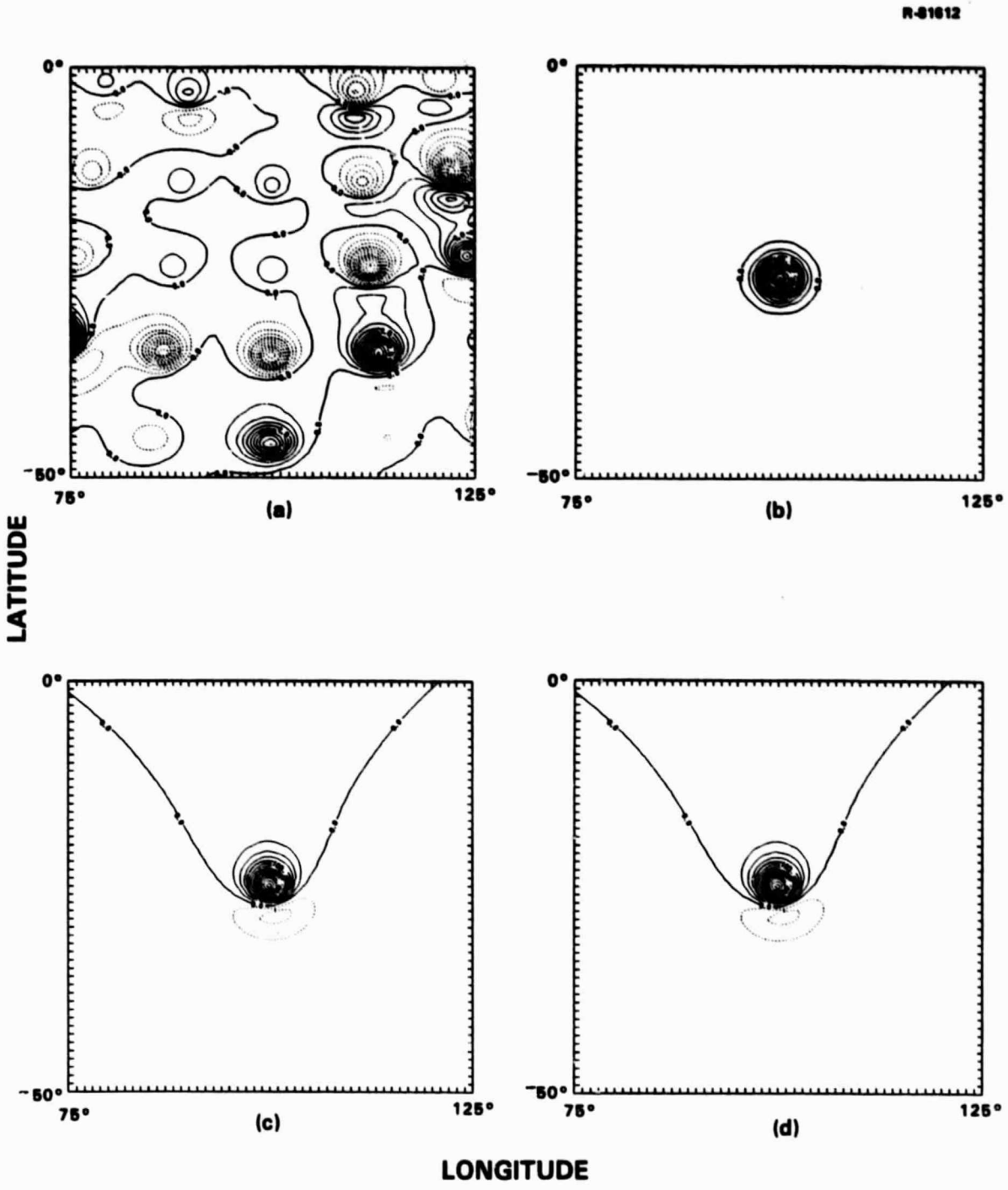

Figure 4-1 Results of ESMAP tests: a) a 25 dipole fit to 3621 data points; b) a 1 dipole fit to the result computed in (a), the output field is reduced to the pole; c) same as (b) but not reduced to the pole; d) a 25 dipole fit to the result computed in (c). Contour interval: 0.25 nT.

value which is not geophysically significant. However, this particular dipole was used to test the internal consistency of ESMAP. After solving for the dipole parameters, the dipole was rotated to a vertical position, and its field computed (Fig. 4-1b). The resulting field shows that the reduction to the pole worked correctly. The computed magnetization parameter and the field are in a form which can be verified in a straightforward manner using standard far-field formulas for a simple dipole. This verification requires conversion of the magnetization parameter to a dipole moment in the appropriate units, and will have geophysical significance when related to the magnetic susceptibility of the local rock (Section 4.5).

Figure 4-1c shows the resulting field when the dipole is not reduced to the pole. The resulting fields are consistent with those expected from a single dipole field. The shape distortion from the input field is due to the use of a single dipole, and the large field magnitude is due to the attempt to fit the magnetization parameter of a single dipole to relatively large values (10 nT) of the field far from the dipole. This is an extreme case of using an insufficient number of dipoles to fit the input field data, as can be seen in the unrealistic value for the magnetization parameter, and an obviously poor fit to the input magnetic field model.

4.2.3 Test 3: Leakage Among Modeled Dipoles

A final consistency test was performed by using the computed field shown in Fig. 4-1c as the input data, and solving for a matrix of 25 dipoles, the center one being located at the same location as the single dipole of Test 2. The dipoles in this case have a 10-degree spacing. The resulting field is shown in Fig. 4-1d, and is visually indistinguishable from Fig. 4-1c. The value of the magnetization parameter of

the centered dipole is 25 times the value of the single dipole (as the volume is 25 times smaller), and the surrounding 24 dipoles have magnetization parameter values more than 5 orders of magnitude smaller than the value for the central dipole. Thus ESMAP is a self-consistent program to generate gridded anomaly fields and does not significantly "leak" magnetization from dipole to dipole.

4.3 ANOMALY MAP RESULTS FOR BROKEN RIDGE AREA

Since ESMAP is limited to solving for a maximum of 150 dipoles on a single run, the first application was to a portion of the investigation region surrounding Broken Ridge.

Maps were produced for several geophysical parameters in the Broken Ridge area: 1) A magnetic anomaly map with approximately 2 degree dipole spacing (Fig. 4-2). This map is reduced to the pole and shows evidence of the grid of dipoles (ripple effect). 2) Bathymetry with 250 meter contours (Fig. 4-3). 3) Gravity anomaly map with 2.5 mgal contours (Fig. 4-4). 4) Geoid Undulation map with 2.5 meter contours (Fig. 4-5).

A magnetic high is evident in the magnetic anomaly map at the eastern (but not the western) end of Broken Ridge, with evidence of a low just south of the high. Two possible interpretations include:

1) Induced magnetization variations, caused by variations in rock composition, or, 2) A large structure having remanent magnetization.

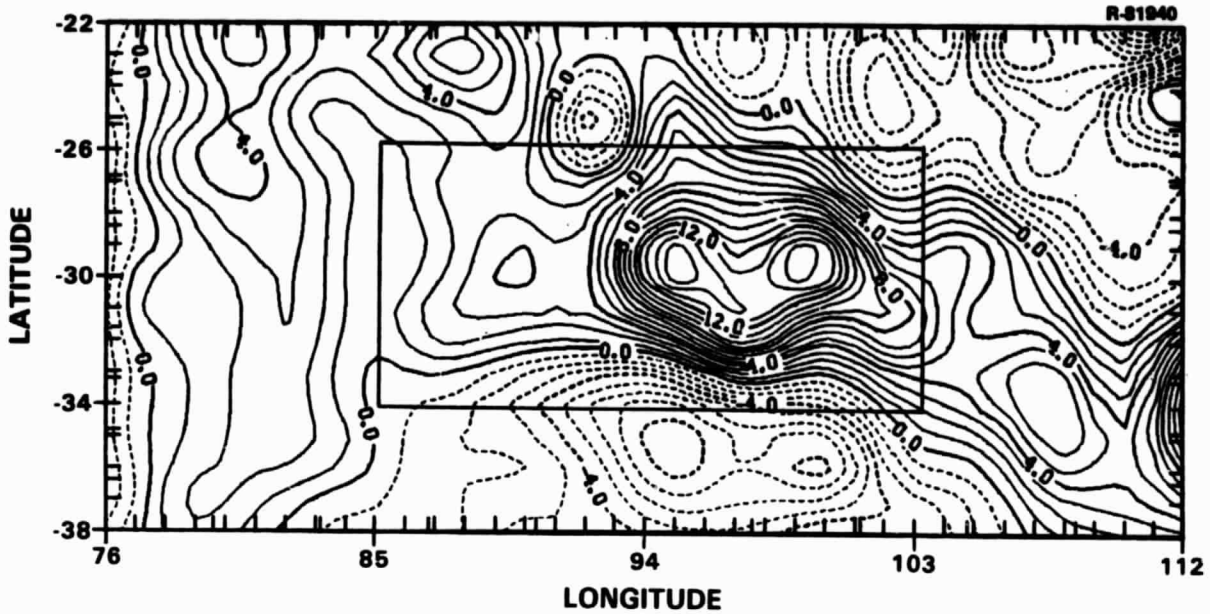

Figure 4-2 Detailed magnetic anomaly map for the Broken Ridge. Anomaly values outside of inset box may be contaminated by edge effects. Contour interval: 1 nT.

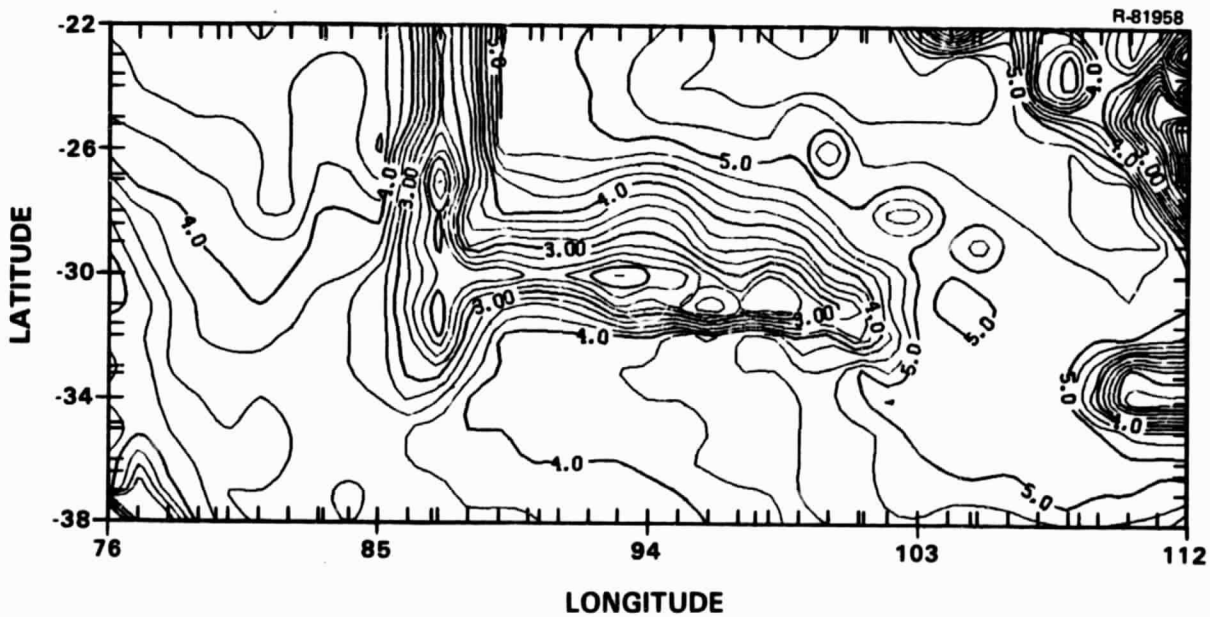

Figure 4-3 Bathymetry for Broken Ridge. Contour interval: 250 meters.

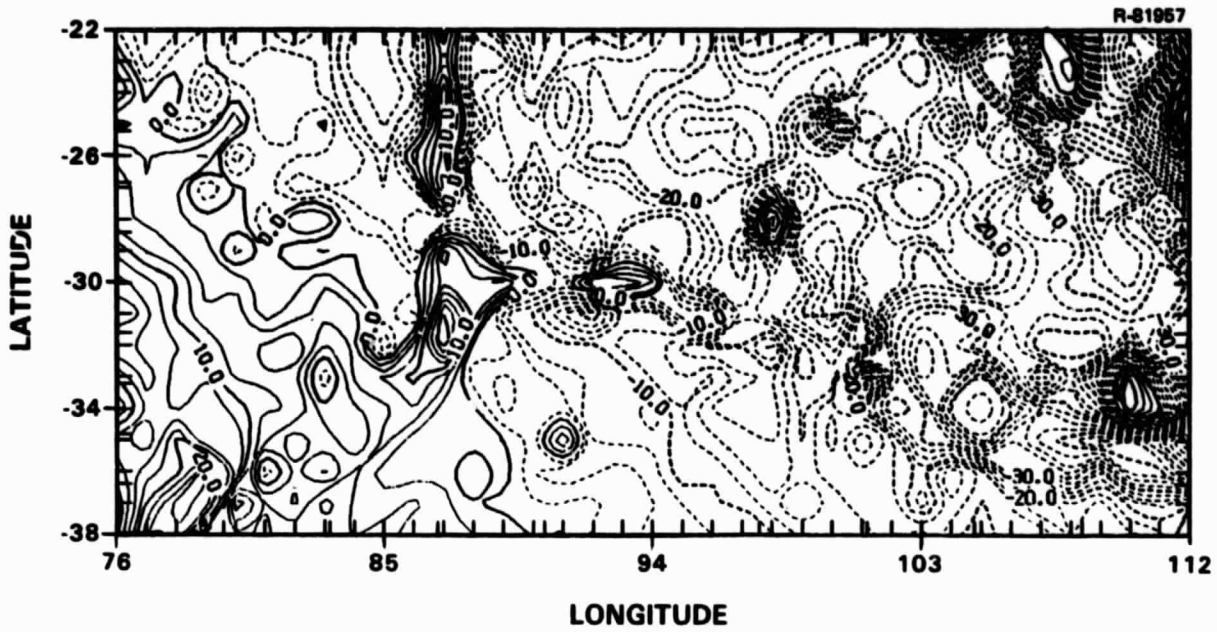

Figure 4-4 Map of gravity anomalies for Broken Ridge. Contour interval: 2.5 mgal.

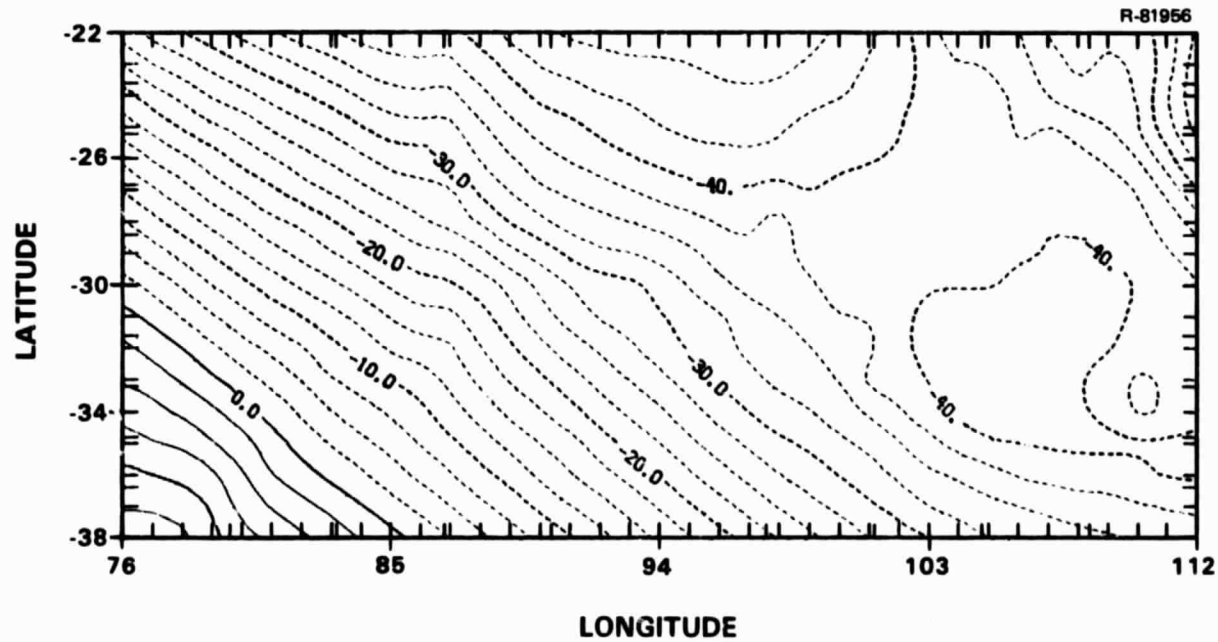

Figure 4-5 Map of geoid undulation for Broken Ridge. Contour interval: 2.5 meters.

It is important to note that the original Magsat data was preprocessed by removing a mean and ramp for each Magsat track. These were removed to minimize effects of external currents and fields. If there were regional trends in the crustal anomaly field over the entire investigation area, these trends would also be removed. If this were the case, the relative anomaly magnitude between small features in different parts of the area would be altered. For example, if the actual crustal anomaly field were tilted to the north, removal of this trend would enhance negative features toward the south, and positive features toward the north. The existence of such a systematic error has not been established, but could give rise to apparently inclined dipoles in maps reduced to the pole.

Visual inspection of the various maps results in the following observations:

- The eastern end of the Broken Ridge does not correlate with a gravity high
- The western end of the Broken Ridge, connecting with the Ninetyeast ridge, is associated with a gravity high, and possibly a small magnetic high. This connecting part does not have the same magnetic properties as the eastern end of the Broken Ridge
- The southern part of the Ninetyeast Ridge is not associated with a major magnetic anomaly, but is associated with a gravity high.

A preliminary conclusion based on these observations suggests that the Broken Ridge consists of two areas with differing crustal properties. The western portion shares similar gravity and magnetic anomaly properties with the Ninetyeast Ridge, and thus may be part of the same geologic feature.

The eastern portion of the Broken Ridge appears to be a separate geological entity from the western section and the Ninetyeast Ridge.

4.4 FINAL EQUIVALENT SOURCE ANOMALY MAP OF STUDY REGION

The analysis of individual tracks of Magsat data showed that crustal anomaly features with wavelengths greater than 700 km were repeatable between nearly coincident tracks of data (Section 3.3, and Ref. 11). Anomaly features with wavelengths between 300 and 700 km were not coherent between closely-spaced tracks, but may have enough power to be above the noise level in the data. Thus, reasonable grid spacings for constructing Magsat anomaly maps would range between 1.5 and 4 degrees. A spacing of 2-deg was chosen for maps of the eastern Indian Ocean since it represents a lower bound on the resolution of the data, and since 2-deg spacing was also used by NASA in constructing a global Magsat anomaly map.

The final equivalent source anomaly map is based on multiple runs of ESMAP using 16 overlapping 20 × 20 deg subregions. Multiple runs were necessary to achieve the desired 2-deg dipole spacing and to minimize edge effects. Figure 4-6 shows the pattern of the 16 subregions that form the final anomaly map. Each of these regions is the central 10 × 10 deg square from the 20 × 20 deg square used in each inversion. The results in the outer 5-deg edges of each 20 × 20 deg square were ignored because of obvious edge effects. The final map covers the central 40 × 40 deg portion of the investigation region using 676 dipoles (including those that nearly overlap).

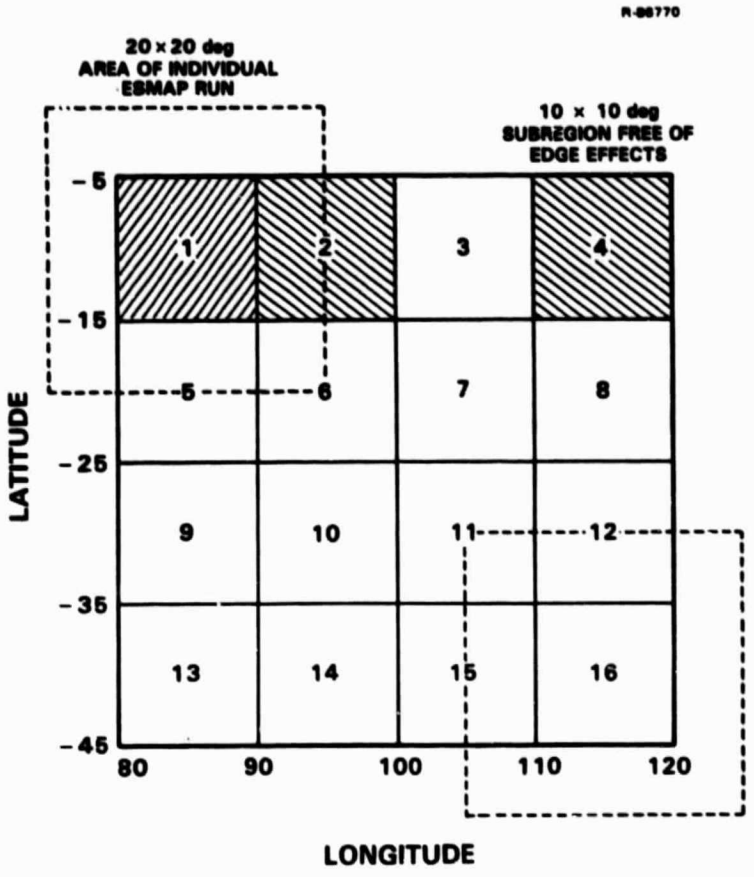

Figure 4-6 Diagram of 16 ESMAP runs used to produce final anomaly map. Dashed lines indicate regions ignored because of edge effects

The output from the separate runs of ESMAP was expressed as a magnetic anomaly map at 350 km altitude, sampled at 1-deg uniform grid spacing (note that the dipoles for each run were spaced at approximately 2-deg and located according to separate equal-area projections). To form the final map of the entire area, the 5-deg boundaries from each 20 × 20 deg sub-map were deleted and the sub-maps were placed together. The sub-maps still overlapped along one row or column of grid points at the edges, and at those locations, the anomaly values were averaged (discrepancies were all <1 nT). A contoured version of the final anomaly map is shown in Fig. 4-7. Figure 4-8 compares the new map, which was reduced-to-the-pole by

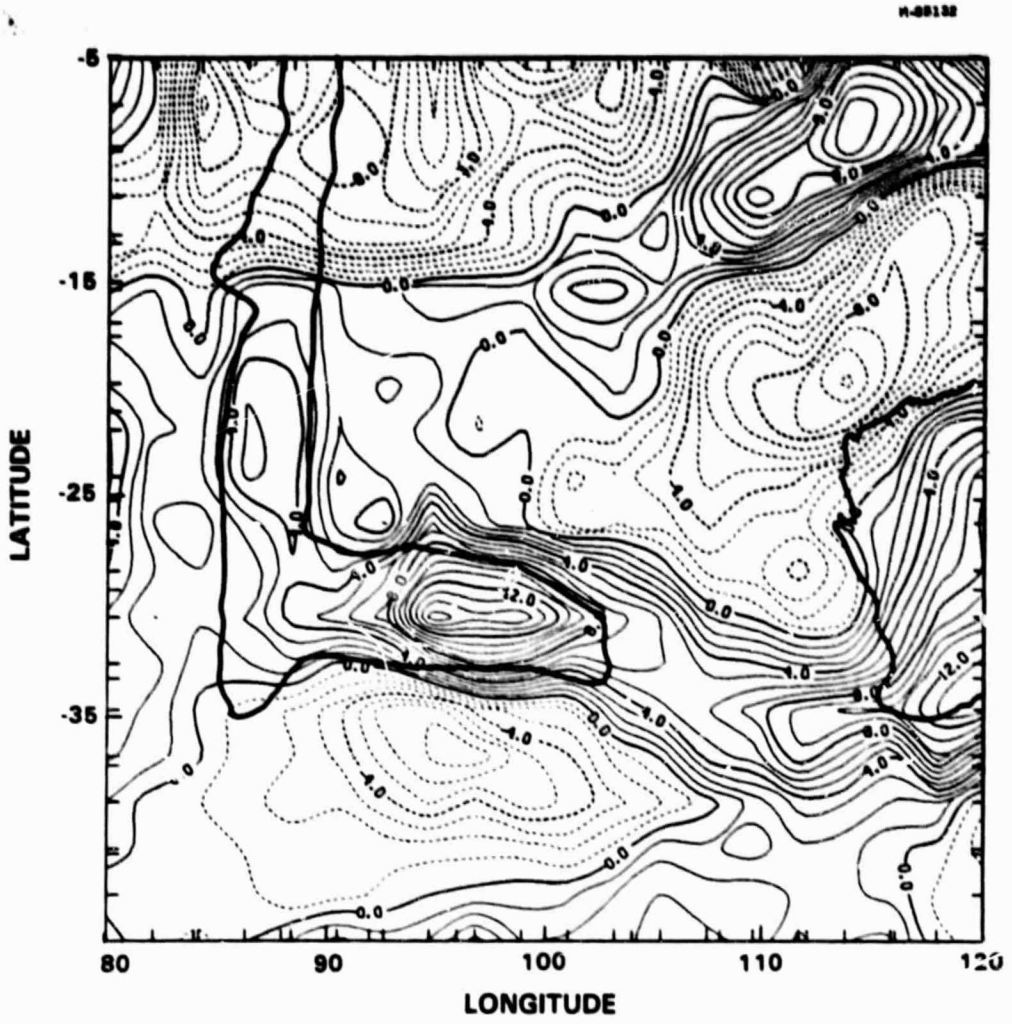

Figure 4-7 Final equivalent-source anomaly map at 350 km from 16 runs of ESMAP. Contour interval: 1 nT.

the ESMAP runs, with the NASA Magsat anomaly map derived by averaging observations in 2-deg bins. The two maps agree in general, but the TASC map shows more definition of the Ninety-east Ridge. Also, the TASC map shows more clearly the presence of a magnetic high trending NE-SW near the NE corner of the investigation region. This magnetic anomaly ridge seems to be correlated with bathymetric trends (see Figs. 1-2 and 4-7).

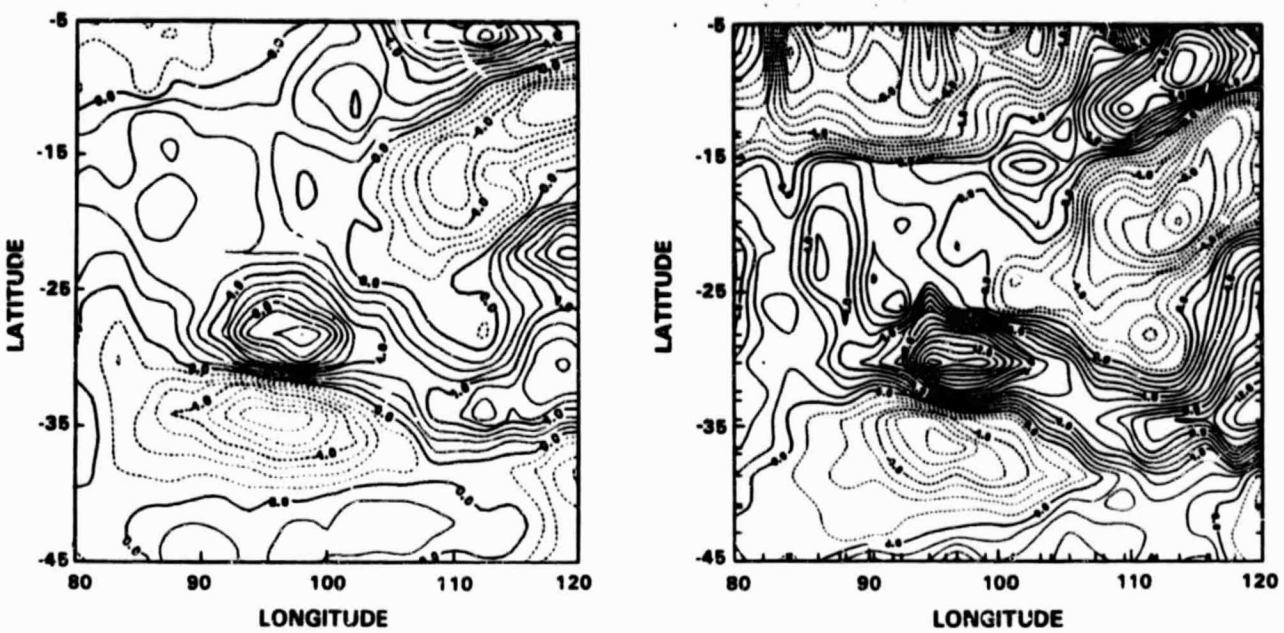

(a) (b)

Figure 4-8 Comparison of TASC and NASA maps: (a) NASA 2×2 deg anomaly map, and (b) new equivalent source map reduced-to-pole (same as Fig. 4-7)

4.5 CRUSTAL MAGNETIZATION AND SUSCEPTIBILITY MAPS

Figure 4-9 is the map of relative magnetization based on the equivalent-source dipole solutions described in Sections 4.2 and 4.4. This map was constructed using the values of dipole moments per unit volume from the 16 ESMAP runs. These were regridded by Lagrange interpolation to form a uniformly spaced 1-deg grid. The contour map is of relative magnetization in the arbitrary units used in the ESMAP software. Broken Ridge, the coast of Australia, the Java Trench area, and part of the Ninetyeast Ridge have relatively high magnetization.

The map of relative magnetization (Fig. 4-9) is useful, but is not expressed in units that can be related to

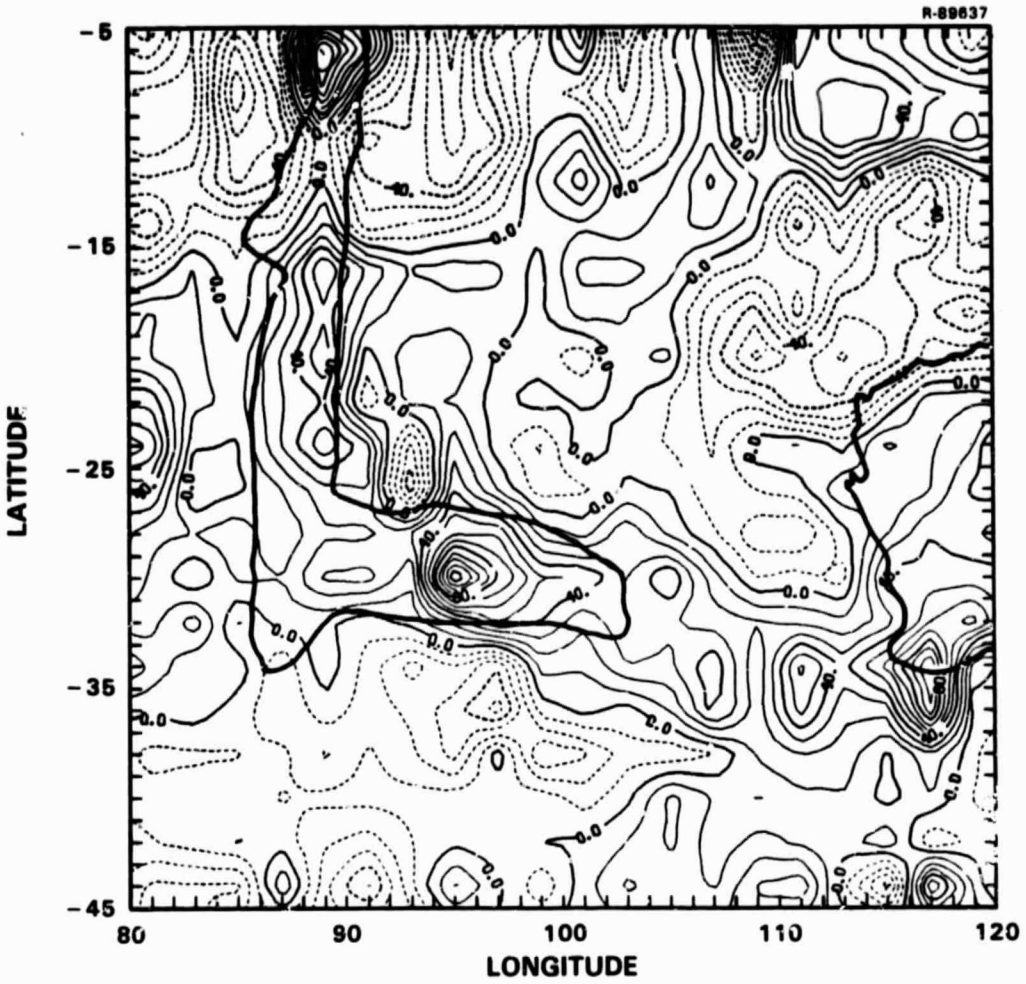

Figure 4-9 Magnetization map showing crustal magnetization anomalies in the arbitrary units of ESMAP

the known physical properties of rocks. For that purpose, a map of magnetic susceptibility was prepared. This requires the assumption that the anomalies computed from the Magsat data are caused by induced magnetization. The method for computing the susceptibility map is described below. The mapped values of susceptibility were expressed in cgs units in order to be comparable to the published results of laboratory studies using rock samples.

The program ESMAP computes magnetic moments (per unit volume) for the model dipoles, and these represent anomalous crustal magnetization. The units used in ESMAP are arbitrary (Ref. 15), apparently chosen for ease of computation. Because information was not available on the units used in ESMAP, an empirical approach was followed to find the units conversion scale factor for susceptibility computations.

A general relation between magnetization and on-axis field is

$$B_z = \frac{P \times Vol}{z^3} \qquad (4\text{-}2)$$

where B_z is the field strength, P is magnetization, Vol is the volume that is uniformly magnetized (represented by a dipole), and z is the distance from the dipole to the observation point. In using Eq. 4-2, ESMAP computes P in arbitrary units which are converted to cgs units using

$$I = C_1 P \qquad (4\text{-}3)$$

where I is magnetization in cgs units, P is the ESMAP magnetization value, and C_1 is the proportionality factor. Applying Eqs. 4-2 and 4-3 to the model dipole tests described in Section 4.2, C_1 has been empirically determined to be

$$C_1 = 2.192 \times 10^{-2} \qquad (4\text{-}4)$$

This empirical factor is not a recognizable combination of conversion factors or permeability constants, but arises from the choice of input units and crustal volume computations in ESMAP.

Assuming the determined values for magnetization in this area are from induced magnetization, then the susceptibility is defined by

$$K = I/B_z \qquad (4\text{-}5)$$

where K is susceptibility in cgs units, I is magnetization in cgs units, and B_z is the inducing (earth's ambient) field in gammas. This equation was used to map susceptibility in the study area. The magnetization I is from the rescaled ESMAP magnetization map. The inducing field B_z was computed from the geomagnetic field model MGST(4/81-2), shown in Fig. 4-10. The resulting map of relative susceptibility, in cgs units, is given in Fig. 4-11. The susceptibility map of Fig. 4-11 represents another way of expressing the relative magnetization results of ESMAP. As with the magnetization map, the location of the zero contour is somewhat arbitrary, since linear trends were removed from the input passes of Magsat data. Thus, while the susceptibility map does show values that are reasonable for terrestrial rocks, it also has negative values because it is a map of a relative quantity. It shows the susceptibiiity variations relative to some arbitrary baseline value.

The geophysical significance of the two-dimensional results presented in this chapter are discussed in the next. To aid this interpretation. bathymetry and gravity data have been used.

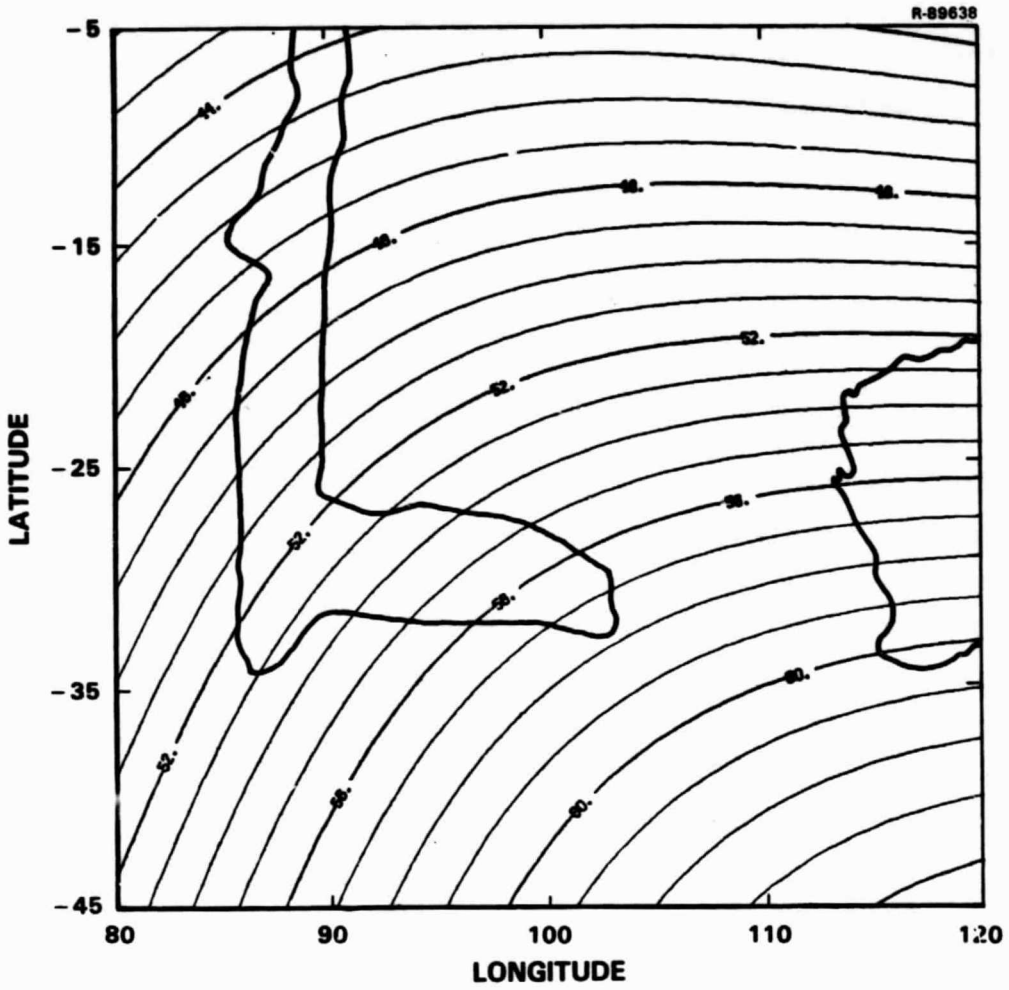

Figure 4-10 Earth's magnetic Field |B| (in units of 1,000 nT) in the investigation area from NASA Field Model MGST(4/81-2) (Ref. 2)

4.6 SUMMARY OF TWO-DIMENSIONAL ANALYSIS

The following points summarize the results of two-dimensional (map) analysis of crustal magnetic anomalies in the eastern Idian Ocean:

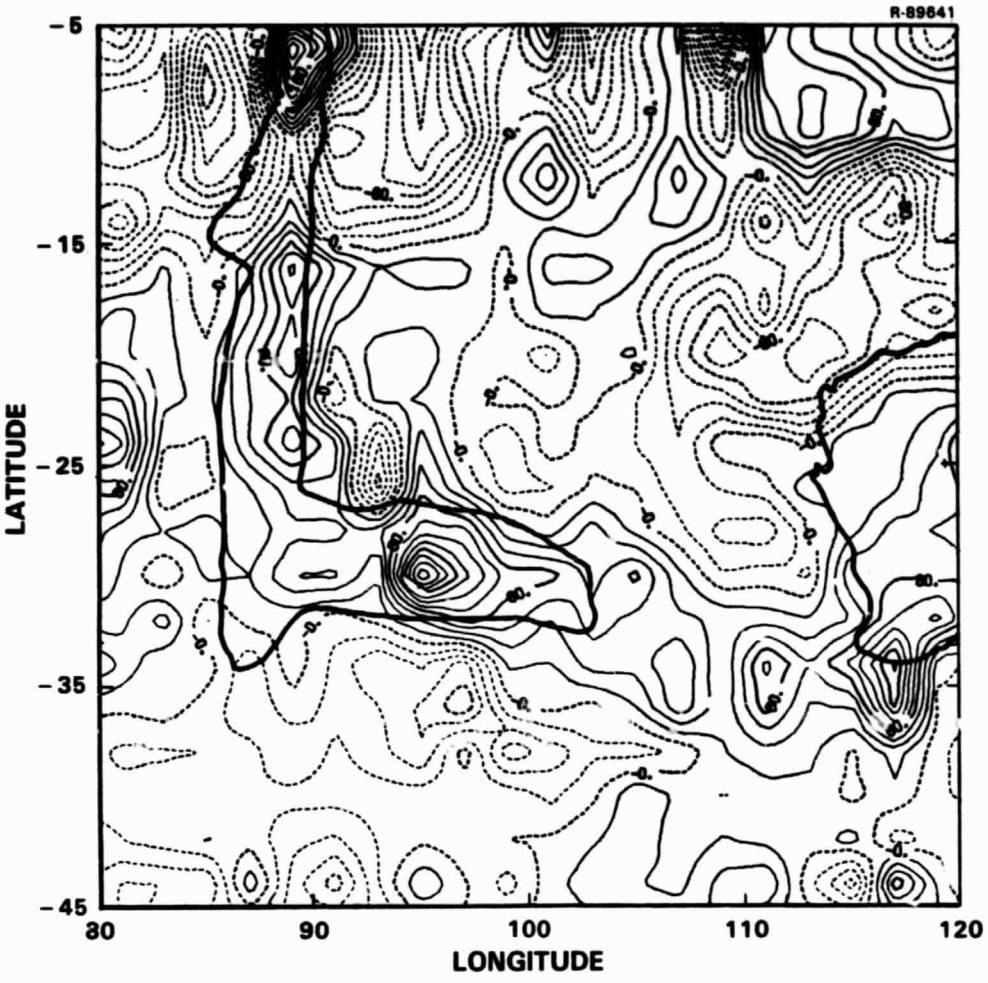

Figure 4-11 Crustal susceptibility anomaly map (multiply contour values by 10^{-6} to get cgs units.)

- A two-dimensional survey simulation was developed to illustrate the effect of satellite altitude on the accuracy of recovering crustal anomalies
- The ESMAP software of NASA was tested and used to compute equivalent source dipoles based on Magsat data covering the investigation region

- Before the equivalent-source computations were performed, data profiles were edited, spikes were removed, and a linear trend was removed from each track. The detrended data were averaged using a moving window five data points wide, to increase the sample interval from 36 km to approximately 180 km

- The following maps were produced using the equivalent sources derived from Magsat data:

  - Magnetic anomaly at 350 km altitude for the Broken Ridge area

  - Magnetic anomaly at 350 km altitude (based on 16 ESMAP runs to reduce edge effects) for the central 40 deg × 40 deg portion of the investigation area

  - Relative crustal magnetization for the 40 deg × 40 deg region

  - Relative crustal susceptibility for the 40 deg × 40 deg region.

5. GEOPHYSICAL INTERPRETATION

This chapter describes geophysical interpretation of the Magsat magnetic anomaly maps. These interpretations are aided by bathymetry and gravity data described in Section 5.1. Section 5.2 describes how the Magsat maps are combined with gravity data to produce a new product -- a map of the ratio of anomalous magnetization to anomalous density.

5.1 BATHYMETRY AND GRAVITY DATA

The bathymetry of the investigation region was shown in Fig. 1-2. This data is from a global data set with 1-deg resolution provided by Prof. Richard H. Rapp, and based on values compiled by the Defense Mapping Agency.

A gravity data base, also provided by Prof. Rapp was also available with 1-deg resolution. Figure 5-1 is a contour map of the 1-deg gravity anomaly at zero altitude. For comparison with the Magsat observations, the gravity field was upward continued to an altitude of 350 km. This was done in spherical coordinates using a set of spherical harmonic expansion coefficients (to degree and order 180) that were also provided by Prof. Rapp (Ref. 19). The gravity anomaly field computed at 350 km altitude is shown by Fig. 5-2.

The vertical derivative of the anomaly field, at 350 km altitude, is shown by Fig. 5-3. This quantity was also computed from spherical harmonic coefficients and it will be used in the Poisson's relation computations described in the next section. Relative to Fig. 5-2, this map shows better correlation with structural features (e.g., Ninetyeast Ridge).

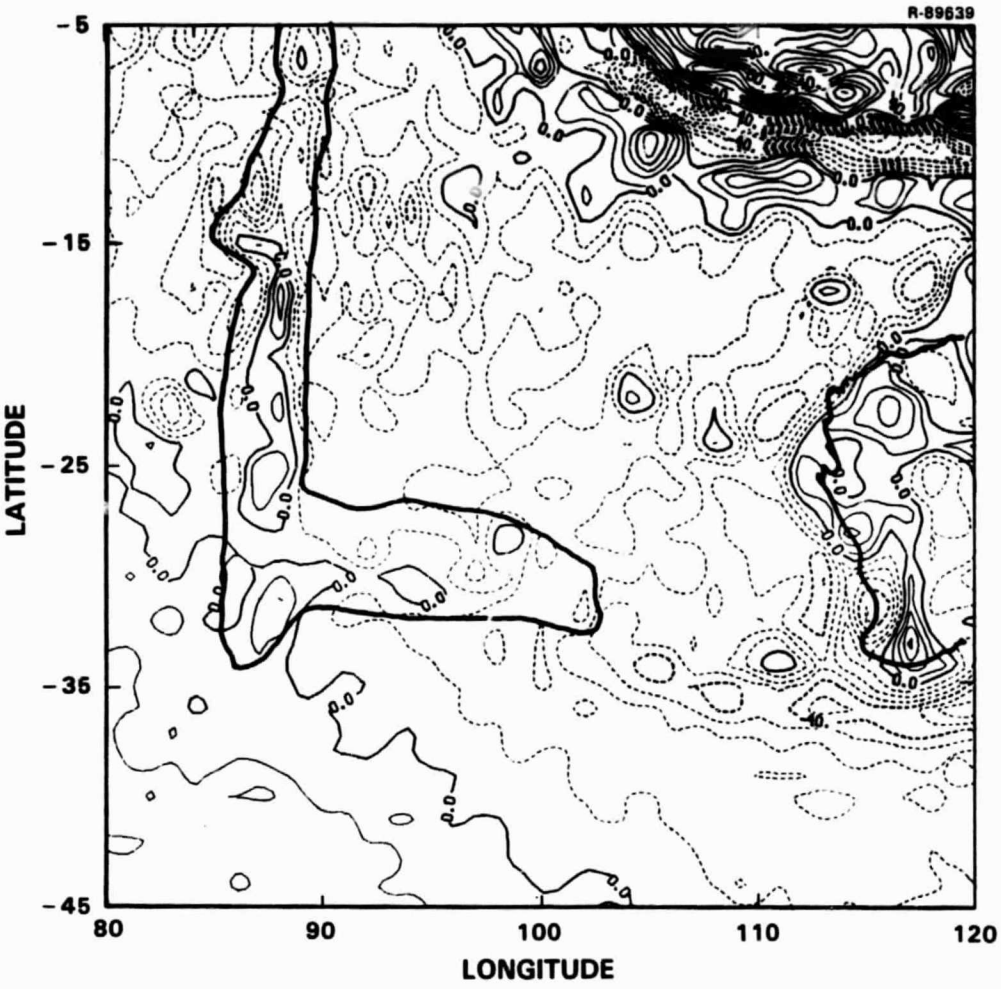

Figure 5-1 Gravity anomaly map at sea surface.
Contour interval: 10 mgal

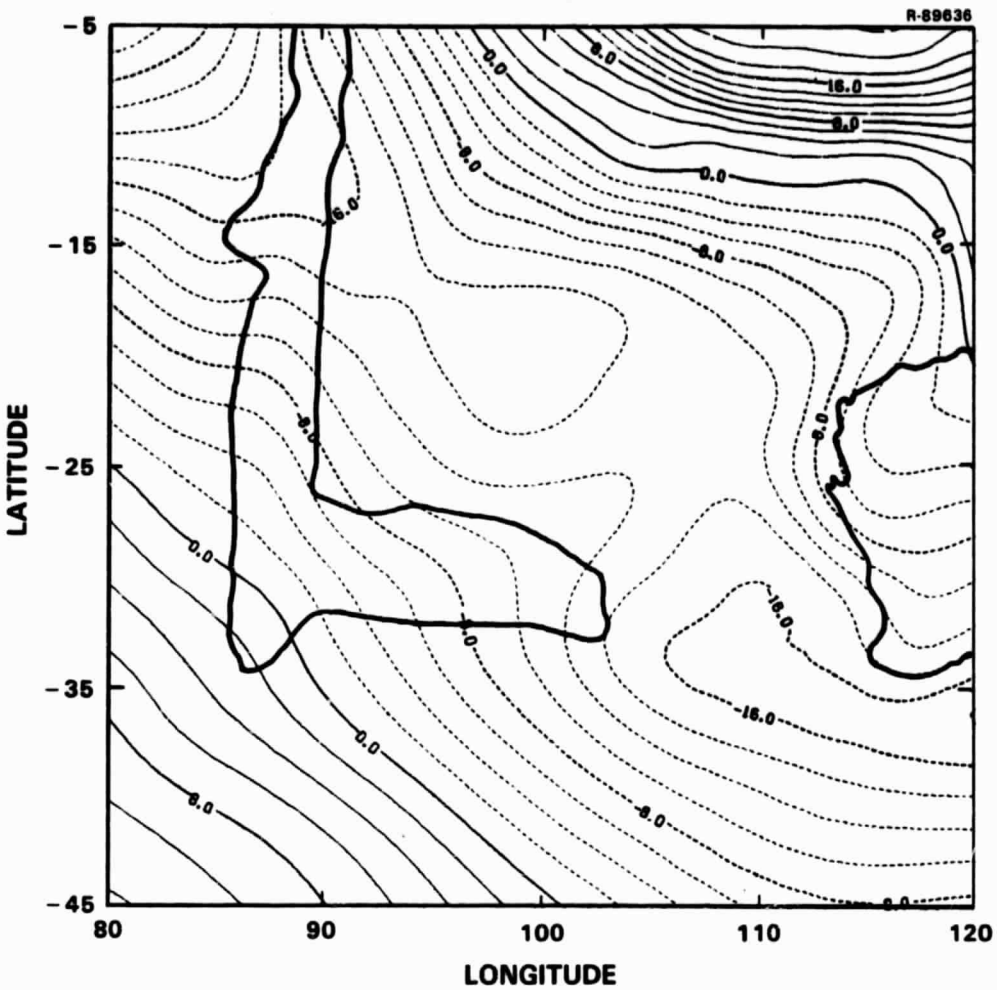

Figure 5-2 Gravity anomaly map at an altitude of 350 km. Contour interval: 2 mgal

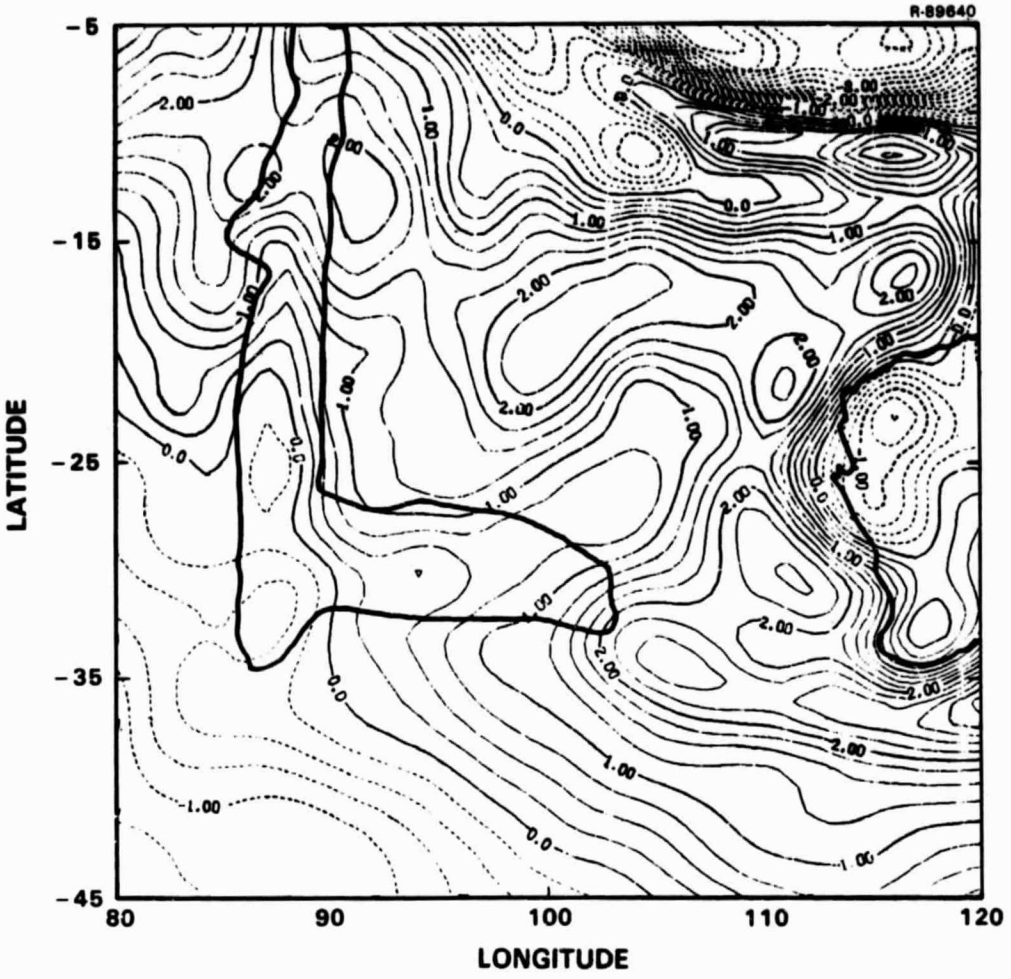

Figure 5-3 Vertical derivative of gravity anomaly at an altitude of 350 km. Multiply contour values by 10^{-5} to get mgals/meter.

5.2 APPLICATION OF POISSON'S RELATION

Understanding the interrelationships among different and/or independently derived geophysical data can lead to better geophysical models. Poisson's relation is an analytic relationship between gravity and magnetic fields which can, with proper interpretation, allow better understanding of the magnetic and density contrasts within the investigation region. Poisson's relation is

$$V = \frac{J}{\rho G} \frac{\partial U}{\partial i} \qquad (5\text{-}1)$$

where V = magnetic potential, J = magnetization contrast, ρ = density contrast, G = gravitational constant, U = gravity potential, i = direction of magnetization. Poisson's relation says that given constant and uniform values for J and ρ, then $\partial U/\partial i$ is proportional to V. If both $\partial U/\partial i$ and V are already known, then Eq. 5-1 can be solved for the ratio J/ρ. Although a varying J/ρ violates a principal assumption of Poisson's Relation, values of J/ρ computed from known U and V are considered to have geophysical significance (Refs. 20 and 21) and can be a measure of variations in J, ρ, crustal thickness, and/or errors in the determination of direction i.

Assuming that the magnetic anomaly field has been reduced-to-the-pole (that is, i is vertical), Eq. 5-1 may be differentiated with respect to the vertical direction z to yield

$$B_z = \frac{J}{\rho G} \frac{\partial g_z}{\partial z} \qquad (5\text{-}2)$$

where B_z is the magnetic field reduced-to-the-pole, and g_z is the vertical component of the anomalous gravity field. For the purpose of computation, the latter is approximated by the gravity anomaly.

To compute a map of the ratio J/ρ, the maps B_z and $\partial g_z/\partial z$ shown in Figs. 4-7 and 5-3 were used. The B_z map was divided by the $\partial g/\partial z$ map, scaled by the universal gravity constant, and scaled to cgs units. The resulting J/ρ map computed using Eq. 5-2 is shown in Fig. 5-4. The main feature evident in this map is that J/ρ is generally constant in the investigation area, suggesting that Poisson's relation applies

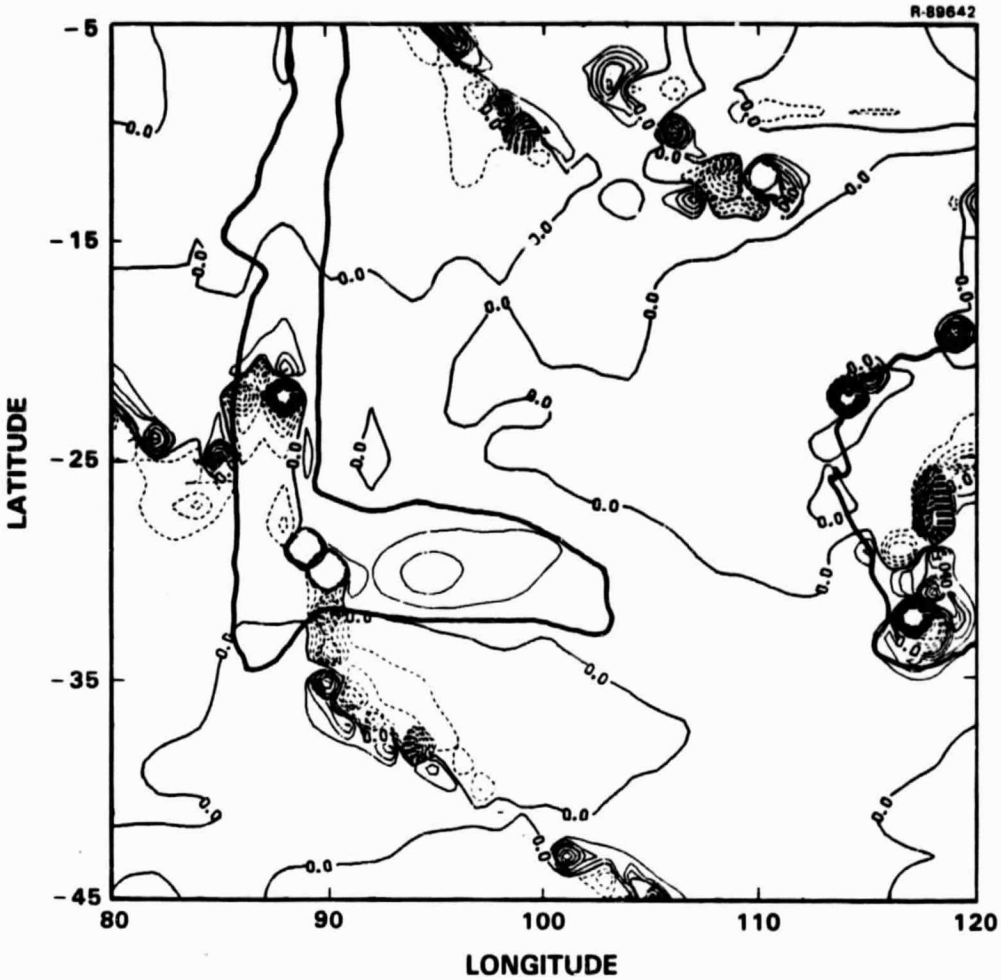

Figure 5-4 Map of J/ρ using Poisson's relation and maps shown in Figs. 4-7 and 5-3. Minimum value: -1.6×10^{-6}, maximum value: 0.7×10^{-6} cgs units.

over most of this area. (Note that since both J and ρ are contrasts relative to an arbitrary baseline, negative values of J/ρ do occur.) Principal deviations in J/ρ are significant lows over western Australia, a feature SW of and parallel to the Java Trench, and a major trend crossing several features in the SW of the map area.

The most prominent feature of the J/ρ map is the strong linear trend, consisting mostly of negative J/ρ, but interlaced

with a few highs, generally parallel and just south of the Diamantina Fracture Zone. A similar trend, likewise oriented, may be a western extension of the feature just NW of the junction of the Ninetyeast Ridge and Broken Ridge. If these two are related, then the northward offset at the Ninetyeast Ridge must have geophysical significance. It is interesting to note that north of this J/ρ offset, the Ninetyeast Ridge has a significant gravity anomaly, and south of this perturbation it does not (Fig. 5-1). Similarly, along the Broken Ridge east of this J/ρ trend, there is a strong magnetic anomaly, and to the west there is not (Fig. 4-7). This linear J/ρ feature thus appears to coincide with the boundary between the northern and southern parts of the Ninetyeast Ridge as well as the boundary between the Broken Ridge and the Ninetyeast Ridge. This suggests that the Ninetyeast Ridge, the Broken Ridge, and the region at the junction of the two have distinct geologic and tectonic characteristics. In fact, geologic maps based on deep-sea drilling show that the Broken Ridge (Upper Cretaceous) is older than either the southern (Eocene) or northern (Paleocene) parts of the Ninetyeast Ridge (Ref. 22).

5.3 RELATIONSHIPS AMONG MAGNETIC AND GRAVITY MAPS

The J/ρ map, constructed from the magnetic anomaly and gravity gradient maps, reflects the combination of changes in average crustal density or magnetic properties. A geographic variation in the ratio J/ρ could be caused by 1) variations in crustal thickness or density, (both of which change the effective average crustal density) or, 2) variations in the crustal magnetization or depth to the Curie isotherm. Effects of the first type would be visible in gravity data products, and effects of the second type would be expressed in the products derived from magnetic observations. There could be situations where both of these effects might occur simulataneously.

The long linear trend in the southwestern part of the J/ρ map is probably caused by some sort of crustal density or thickness change, because it is correlated with the gravity anomaly maps. This feature is correlated with the zero contour of the vertical gravity gradient (Fig. 5-3) and to some extent with the zero mgal anomaly contour (Fig. 5-1). Since the J/ρ map was computed by dividing the magnetic anomaly by the gravity gradient at each map grid point, large magnitude values of J/ρ occur at points where the gradient is small in magnitude. This computational process did not diverge because there were no grid points where the gradient was exactly equal to zero. This feature on both the gradient and J/ρ maps probably does indicate a significant and deep-seated crustal feature.

Since values of J/ρ do not vary greatly over the rest of this map, and especially do not change drastically over the Broken Ridge or Ninetyeast Ridge, it is probable that those tectonic features are associated with magnetic anomalies mainly because they have thicker crust, as is reflected in the bathymetry. However, further work is necessary to determine whether changes in rock composition and a higher bulk susceptibility could also account for the observed magnetic anomaly features.

The magnetic anomaly, magnetization, and susceptibility maps are correlated with one another and with bathymetry. All three of these maps are based on the same set of equivalent source dipoles and thus (to varying degrees, depending on units and other scaling) all show the same degree of correlation with tectonic features. Then, at least for the eastern Indian Ocean, positive magnetic anomalies seem to be associated with older and thicker crust that produces bathymetric highs.

Positive magnetic anomalies are also associated with the continental crust of Australia and Naturaliste Plateau.

However, it is not yet possible to determine whether or not the bathymetric features such as Broken Ridge might also contain some continental crust. Compared to oceanic crust, continental crust would have a relatively high magnetic susceptibility and could account for the observed magnetic anomalies. Further observations and modeling will be necessary to answer this question.

6. SUMMARY AND CONCLUSIONS

The accomplishments of this investigation include:

- Evaluation of the Magsat data in terms of identification of crustal anomaly features and noise characteristics
- Characterization of spectral features and coherence among different tracks
- Production of magnetic anomaly and susceptibility maps from Magsat data
- Merging Magsat data with gravity data using Poisson's relation.

These results have shown that Magsat data is an important tool for global geophysics. The objectives listed in Chapter 1 have been satisfied, although there are still more questions to be answered.

The Magsat data preprocessing and analysis of the data quality began with the identification and removal of data problems, which include: 1) missing data values, and 2) spikes of about 15 nT. Then, in order to remove or at least minimize the effects of external fields and the core field, a global field model and a mean and ramp were subtracted from each individual track. This preprocessing removed the very long wavelength and very high frequency noise in the Magsat data, leaving a first estimate for the crustal anomaly field. At this point, potentially useful data was in the 1050 to 72 km wavelength range.

Spectral studies were performed to define the wavelength bands in which either crustal anomaly fields or noise dominated the data. Analysis of power spectra and spectral coherence between neighboring tracks, showed that the wavelength range of 1050 to 700 km contains geophysically useful and coherent information; and the 700 to 250 km range contains incoherent (non-repeatable from track to track) information, probably with equal power for the geophysical signal and the noise. The wavelength band from 250 to 72 km is clearly dominated by noise. Given this result, the useful sampling interval can be greatly increased from the value on the Investigator tapes (36 km). An increase of the interval to nearly 125 km would result in a substantial savings in data storage and processing.

After determining the resolution capability from the along-track data, the work turned to two-dimensional (map) questions. A survey simulation was designed to show how accurate Magsat type survey data would be, especially if it were desired to downward continue that data for comparison with aeromagnetic surveys. A table was prepared representing the accuracies at several different satellite survey altitudes.

A primary goal of this investigation was to produce a gridded crustal magnetic anomaly map for the investigation area. This has been accomplished using equivalent source inversion which yielded a map that is an alternative to the standard NASA map. In the new TASC map, certain magnetic anomaly features are more visible (e.g., the small magnetic anomaly in the vicinity of the Ninetyeast Ridge, a NE-SW magnetic "ridge" connecting the eastern end of Broken Ridge with the Java Trench). Certainly one of the reasons for this feature enhancement and/or extra detail is that our map is reduced-to-the-pole, but the major reason is that all the data are numerically reduced

to a common altitude. Very useful byproducts of this processing are maps of crustal magnetization and susceptibility anomalies. The latter directly relates to an important physical property of the crustal material, and is strongly linked with the relative content of magnetic minerals. Since these maps are anomaly maps, ground truth references must be (but have not yet been) made available and used to yield estimates of actual rock properties.

The result that is perhaps the most interesting, but presently the least well-understood, is the joint analysis of gravity and magnetic anomaly data. Poisson's relation combines these two data sets in a map of J/ρ (anomalous magnetization over anomalous density). This map shows that J/ρ is generally uniform over the entire investigation area, with a few exceptions. The major exception is a linear feature of unstable J/ρ values aligning with the Diamantina Fracture Zone and cutting across Ninetyeast Ridge. This feature in the J/ρ map is probably associated with crustal density or thickness properties, but the interpretation of its significance is incomplete. These results merit further investigation as they show the possibilities for developing new approaches to solving problems in crustal geophysics using satellite data.

In conclusion, this investigation yielded results exceeding those outlined in the proposal, but it is only a stepping stone to the types of geophysical analyses possible using these remote sensing techniques. Two-dimensional data processing, including image processing, and analyis of different and complementary geophysical data sets are the next obvious steps. Other recommendations for further work include additional analysis of the correlations between the gravity and magnetic fields in both oceanic and continental areas, in order to determine the source depth for both types of anomaly.

REFERENCES

1. R.D. Regan, J.C. Cain, and W.M. Davis. A Global Magnetic Anomaly Map. Journal of Geophysical Research, Vol. 80, No. 5, February 1975, pp. 794-802.

2. R. Langel, J. Berbert, T. Jennings, and R. Horner. Magsat Data Processing: A Report for Investigators. NASA Technical Memorandum 82160, Goddard Space Flight Center, November 1981.

3. K.W. Hipel. Geophysical Model Discrimination Using the Akaike Information Criterion. IEEE Trans. Automat. Control. AC-26, No. 2, 1981, pp 358-378.

4. F.J. Lowes. Spatial Power Spectrum of the Main Geomagnetic Field, and Extrapolation to the Core. Geophys. J. R. Astr. Soc., Vol. 36, 1974, pp. 717-730.

5. L.R. Alldredge, G.D. Van Voorhis, and T.M. Davis. A Magnetic Profile Around the World. J. Geophys. Res., Vol. 68, 1963, pp. 3679-3692.

6. M.G. McLeod, and P.J. Coleman. Spatial Power Spectra of the Crustal Geomagnetic Field and Core Geomagnetic Field. Phys. Earth and Planet. Int., Vol. 23, 1980, pp. P5-P19.

7. W.G. Heller, and S.K. Jordan. Attenuated White Noise Statistical Gravity Model. J. Geophys. Res., Vol. 84, 1979, pp. 4680-4688.

8. R.V. Sailor. Relationships Between Along-Track and Two-Dimensional Spectra of Geophysical Data: Applications in Geodesy. (Abstract), EOS, Trans. Am. Geophys. Un., Vol. 61, 1980, p. 937.

9. I.S. Gradstyn, and I.M. Ryzik. Table of Integrals, Series, and Products, Academic Press, New York, 1965.

10. A. Spector, and F.S. Grant. Statistical Models for Interpreting Aeromagnetic Data. Geophysics, Vol. 35, 1970, pp. 293-302.

11. R.V. Sailor, A.R. Lazarewicz, and R.F. Brammer. Spatial Resolution and Repeatability of Magsat Crustal Anomaly Data Over the Indian Ocean. Geophysical Research Letters, Vol. 9, April 1982, pp. 289-292.

REFERENCES (Continued)

12. L.H. Koopmans. The Spectral Analysis of Time Series. Academic Press, New York, 1974.

13. G.P. Box, and G.M. Jenkins. Time Series Analysis. Holden-Day, San Francisco, 1976. pp. 575.

14. M.A. Mayhew, B.D. Johnson, and R.A. Langel. An Equivalent Source Model of the Satellite Magnetic Anomaly Field Over Australia. Earth Planet. Sci. Lett., Vol. 51, 1980, pp. 189-198.

15. R.J. Horner, Jr. The Equivalent Source Magnetic Anomaly Program (ESMAP) User's Guide. Prepared by Computer Sciences Corporation for Goddard Space Flight Center, 1980.

16. R.A. Langel, R.L. Coles, and M.A. Mayhew. Comparisons of Magnetic Anomalies of Lithospheric Origin Measured by Satellite and Airborne Magnetometers over Western Canada. Canadian J. Earth Sci., Vol. 17, No. 7, 1980, pp. 876-887.

17. M.G. McLeod, and P.J. Coleman. Geomagnetic Field Mapping from a Satellite: Spatial Power Spectra of the Geomagnetic Field at Various Satellite Altitudes Relative to Natural Noise Sources and Instrument Noise. Phys. Earth Planet. Int., Vol. 23, 1980, pp. 222-231.

18. M. McLeod. Optimal Filtering of Satellite Derived Magnetic Anomaly Data. Phys. Earth Planet. Int., submitted, 1982.

19. R.H. Rapp. The Earth's Gravity Field to Degree and Order 180 Using Seasat Altimeter Data, Terrestrial Gravity Data and Other Data. The Ohio State University, Department of Geodetic Science, Report No. 322, December 1981.

20. L. Cordell, and P.T. Taylor. Investigation of Magnetization and Density of a North American Seamount Using Poisson's Theorem. Geophysics, Vol. 36, 1971, pp. 919-937.

21. E.R. Kanasewich, and R.G. Agarwal. Analysis of Combined Gravity and Magnetic Fields in Wave Number Domain. J. Geophys. Res., Vol. 75, 1970, pp. 5702-5712.

22. B.G. Heezen, R.P. Lynde, and D.J. Fornari. Geologic Map of the Indian Ocean. Amer. Geophys. Union, 1978.